NASA TECHNICAL NOTE

NASA TN D-6490

COMPARISONS OF IN-FLIGHT F-111A INLET PERFORMANCE FOR ON- AND OFF-SCHEDULED INLET GEOMETRY AT MACH NUMBERS OF 0.68 TO 2.18

by Richard A. Martin and Donald L. Hughes

Flight Research Center
Edwards, Calif. 93523

NATIONAL AERONAUTICS AND SPACE ADMINISTRATION • WASHINGTON, D. C. • SEPTEMBER 1971

1. Report No.	2. Government Accession No.	3. Recipient's Catalog No.
NASA TN D-6490		

4. Title and Subtitle
COMPARISONS OF IN-FLIGHT F-111A INLET PERFORMANCE FOR ON- AND OFF-SCHEDULED INLET GEOMETRY AT MACH NUMBERS OF 0.68 TO 2.18

5. Report Date: September 1971

6. Performing Organization Code:

7. Author(s)
Richard A. Martin and Donald L. Hughes

8. Performing Organization Report No.: H-654

9. Performing Organization Name and Address
NASA Flight Research Center
P. O. Box 273
Edwards, California 93523

10. Work Unit No.: 720-52-00-04-24

11. Contract or Grant No.:

12. Sponsoring Agency Name and Address
National Aeronautics and Space Administration
Washington, D. C. 20546

13. Type of Report and Period Covered: Technical Note

14. Sponsoring Agency Code:

15. Supplementary Notes

16. Abstract

Total- and static-pressure data from the left inlet of a prototype F-111A airplane were recorded over a large portion of the aircraft's operating range during automatically scheduled and manually controlled off-schedule positioning of the two-cone compression spike. These data were used to derive inlet performance parameters which indicated that a relatively wide range in performance may be expected during normal operation of an inlet and control system of the type used in this study. In addition, the data showed that the preset controller schedule produced nearly optimum performance for the installation tested. However, significant performance degradation occurred during off-schedule operation. Compressor stalls due to small inlet geometry changes were found to be most likely to occur at high supersonic Mach numbers, and more range in second-cone angle was available before a compressor stall occurred with a blunt-lip cowl than with a sharp-lip cowl. Trends of total-pressure recovery and distortion in flight data were similar to trends in both full-scale and 1/6-scale-model data. Total-pressure recovery obtained during automatic operation of the test inlet compared within about 3 percent of 1/6-scale-model data for predicted optimum inlet geometry.

17. Key Words (Suggested by Author(s))	18. Distribution Statement
F-111A airplane Inlet performance Engine compressor stall Variable geometry inlet	Unclassified - Unlimited

19. Security Classif. (of this report)	20. Security Classif. (of this page)	21. No. of Pages	22. Price*
Unclassified	Unclassified	46	$3.00

*For sale by the National Technical Information Service, Springfield, Virginia 22151

COMPARISONS OF IN-FLIGHT F-111A INLET PERFORMANCE FOR ON- AND OFF-SCHEDULED INLET GEOMETRY AT MACH NUMBERS OF 0.68 TO 2.18

Richard A. Martin and Donald L. Hughes
Flight Research Center

INTRODUCTION

Air inlets for jet engines in aircraft which fly at high supersonic speeds must have controlled variable geometry features to achieve high propulsive efficiency over a wide range of flight conditions. They must meet the airflow needs of the engines with maximum total-pressure recovery and minimum distortion and drag. For such inlets it is important to be able to predict analytically and to verify in wind-tunnel tests and in flight those positions of the movable parts which both optimize inlet performance and assure inlet stability.

Inlet control studies are started early in the conceptual stages of aircraft systems design and are continued as the inlet evolves to its final form. Once the aerodynamic characteristics of the inlet-engine system have been determined from scale-model tests, consistent and predictable control parameters are selected, measurement locations are chosen, and sensors are developed to provide control signals. Despite extensive wind-tunnel testing, flight tests of the full-size inlet are mandatory to determine absolute values of the control signal levels which will yield optimum inlet performance over the flight region. This information is essential to the design of an effective air-induction control system.

During a series of experimental flights of a prototype F-111A airplane conducted by the NASA Flight Research Center, total-pressure data from the left inlet were recorded over a large portion of the aircraft's operating range. The F-111A airplane has an axially symmetric type of external-compression inlet in which the longitudinal position of the two-cone compression spike and the angle of the second-cone ramp are normally automatically controlled by Mach number measurements ahead of and inside the inlet in accordance with a preset schedule. Data were recorded during "on schedule," or "automatic," and manual "off-schedule" inlet geometry settings for selected flight conditions at Mach numbers from 0.68 to 2.18. These tests were part of a more general inlet investigation from which preliminary results were presented in references 1 to 3.

The purpose of this report is to present results showing the effect of automatic and off-schedule positioning of the left inlet spike and second-cone angle on inlet steady-state performance. Off-schedule operation frequently resulted in compressor stalls. Performance data obtained immediately prior to many of these stalls are presented. Also, data are compared, where possible, with wind-tunnel data.

SYMBOLS

Physical quantities in this report are given in the International System of Units and parenthetically in U. S. Customary Units. The measurements were taken in U. S. Customary Units. Factors relating the two systems are given in reference 4.

A	area, m^2 (ft^2)
C	ratio of compressor inlet radius to any radius
D	total-pressure distortion
h	altitude, m (ft)
i	integer variable
j	free index
K_D	total-pressure-distortion factor
M	Mach number
n	number of data samples
p	pressure, kN/m^2 (lb/ft^2)
N_{Re}	Reynolds number, based on cowl lip radius and on free-stream fluid properties
T	temperature, °C (°F)
Tu	turbulence factor
w	airflow, kg/sec (lb/sec)
$\frac{w_2}{w_\infty}$	mass-flow ratio
$\frac{X}{R}$	ratio of distance, X, between inlet cowl lip and spike tip to inlet cowl radius, R, 84.56 cm (33.29 in.)
α	angle of attack, deg
β	angle of sideslip, deg
δ	ratio of local absolute total pressure to absolute total pressure at sea level for a standard day

η	total-pressure recovery, $\frac{p_t}{p_{t,\infty}}$
Θ	ratio of absolute total temperature to absolute total temperature at sea level for a standard day
Θ_{sca}	second-cone angle measured with respect to the center-body axis of symmetry, deg
μ	mean value, kN/m^2 (lb/ft^2)
σ	standard deviation, kN/m^2 (lb/ft^2)
$\bar{\phi}$	largest continuous arc of the ring over which the total pressure is below the ring average, deg
ψ	root mean square, kN/m^2 (lb/ft^2)

Subscripts:

av	average
c	corrected to standard day sea-level conditions
D, E, F, G	cowl lip rake locations
i	compressor face total-pressure-probe ring number
k	location of local Mach probe
L	location of cone static-pressure measurement
M, N, P, Q	locations of inlet duct static-pressure measurements
max	maximum
min	minimum
s	static
t	total
∞	free stream
1	inlet lip station (aft of normal shock)
2	diffuser exit (compressor face) station

APPARATUS

Airplane

An early model (S/N 639771) of the F-111A airplane, a two-place fighter-bomber with variable sweep, high-mounted wings, was used as the test vehicle. Figure 1 is a photograph of the airplane, and figure 2 is a three-view drawing. The F-111A airplane was designed for long-range subsonic cruise, supersonic cruise at low and high altitudes, and had the capability of exceeding Mach 2.0 at 13,700 meters (45,000 feet) altitude. The airplane was powered by two TF30-P-1 afterburning turbofan engines mounted side by side in the aft fuselage. Each engine was rated in the 80-kilonewton (18,000-pound) sea-level static-thrust class.

Inlet System

The inlet system on the F-111A test airplane was representative of one in a series of early inlet design configurations. Although the operating principles and control techniques were the same as those for the production F-111 inlet, the test inlet was a prototype and was, in this sense, unique.

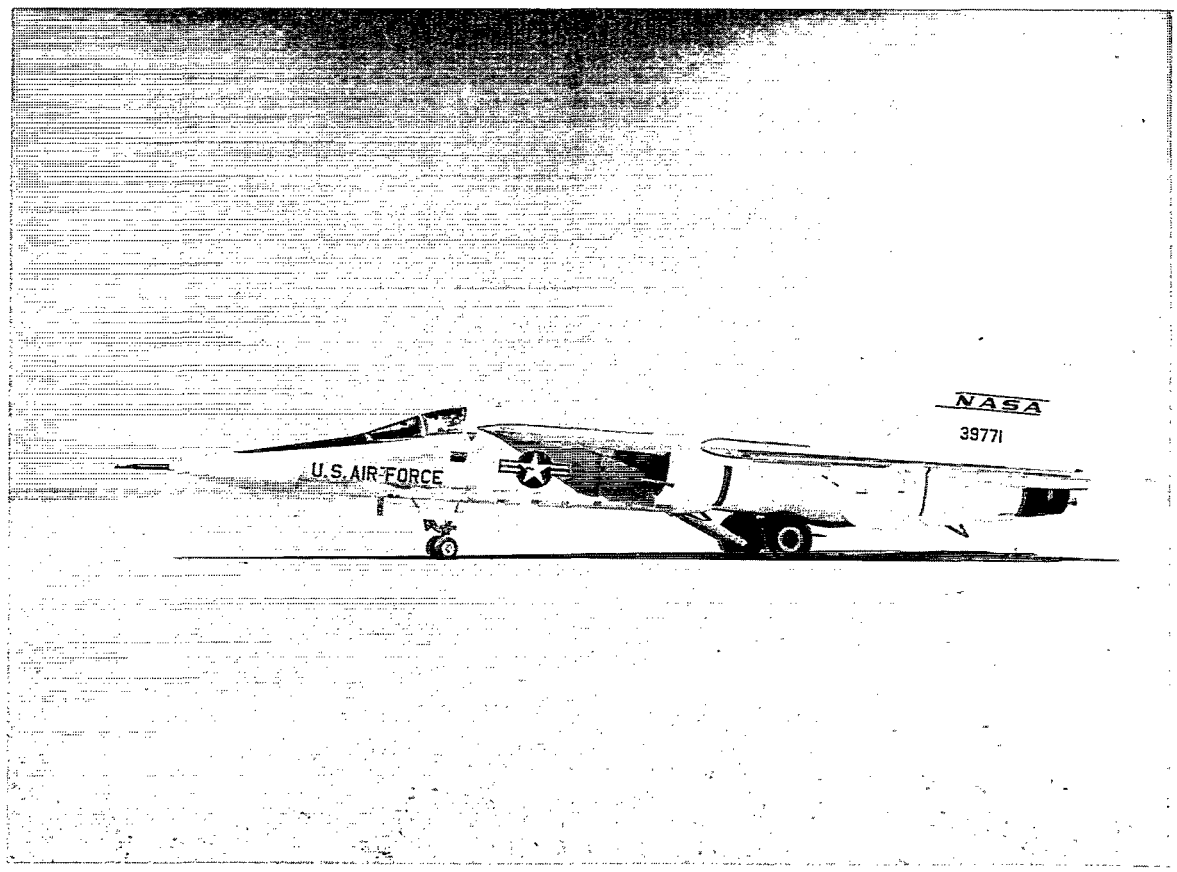

E-20271

Figure 1. F-111A (number 6) airplane.

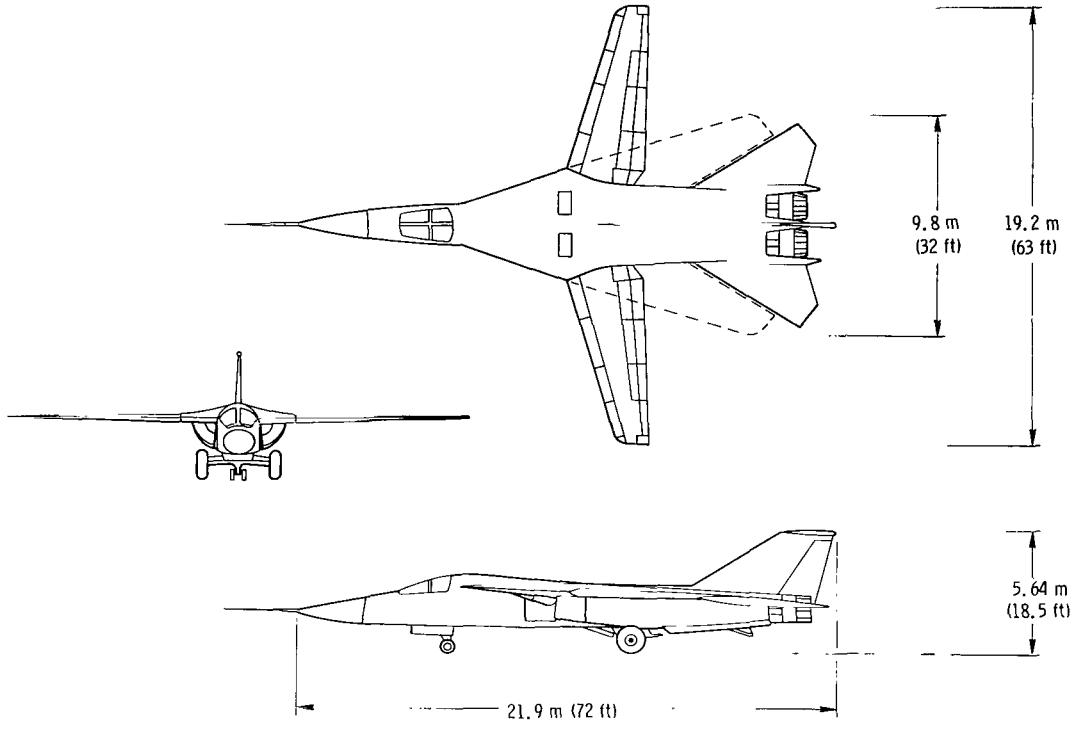

Figure 2. Three-view drawing of F-111A airplane.

The test airplane had two external compression inlets beneath the wing-fuselage junctures (fig. 2). These inlets were approximately quarter-round segments of axially symmetric inlets, and each provided airflow to one of the engines through separate ducts about 4. 11 meters (13. 5 feet) long. The inlets incorporated variable geometry to attain inlet-engine airflow matching and to adjust the amount of compression throughout the operating range. Inlet geometry together with the free-stream Mach number and airflow demand of the engines fixed the position of the compression shock system.

Appendix A describes the two-cone air compression surface or "spike," the devices which were used to prevent low-energy boundary-layer air from entering the inlet, and the internal flow stabilizing devices. Appendix A also describes the differences between the sharp- and blunt-lip inlet cowl configurations used during these tests.

Inlet Control System

Figure 3 is a simplified control signal flow chart for the inlet control system in the test airplane. Spike translation was controlled as a function of local Mach number (ahead of the inlet) and diffuser exit Mach number. This portion of the control included position feedback. Second-cone angle was controlled by the same parameters in a loop which maintained a scheduled shock position pressure ratio. A detailed description of full-scale wind-tunnel testing of a prototype F-111 inlet geometry controller and a discussion of the principles of operation are presented in reference 5.

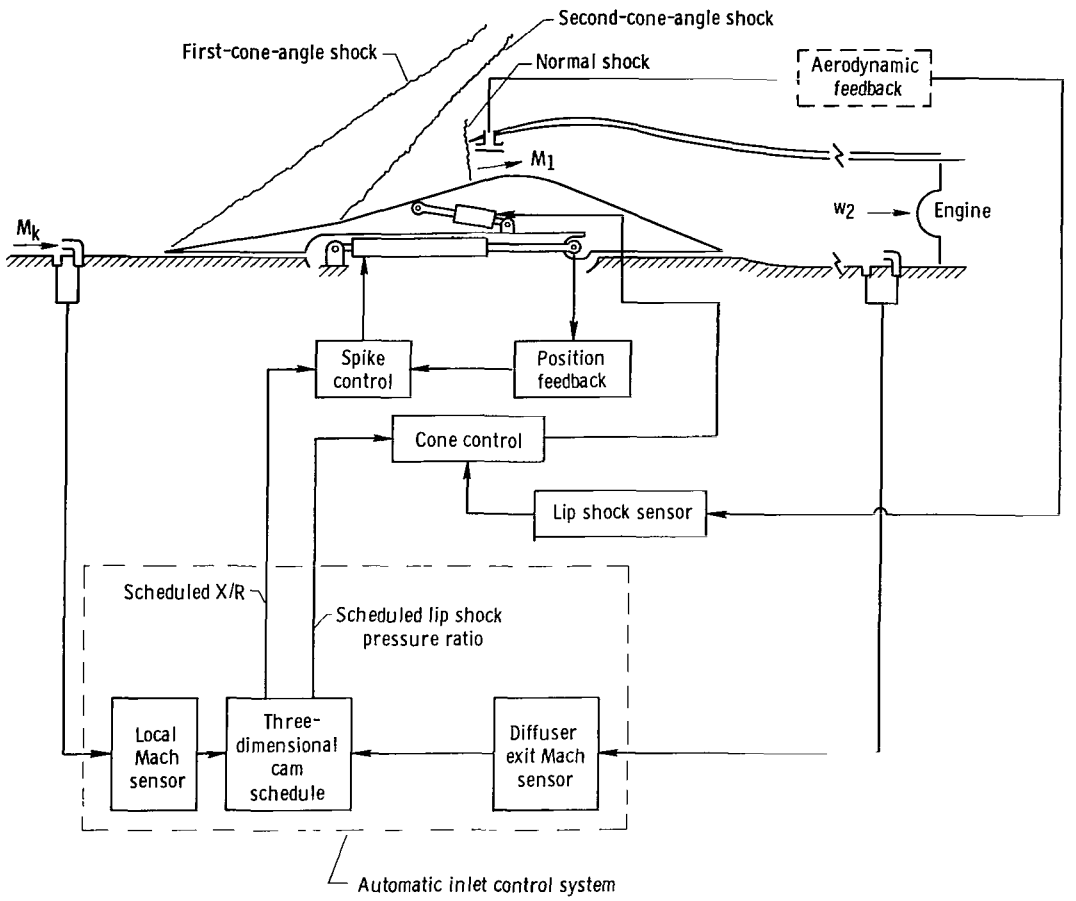

Figure 3. Schematic of inlet control signal flow.

At subsonic and low transonic flight speeds, the inlet spike was normally positioned forward and the second cone fully collapsed by the inlet controller to minimize spillage drag and compression. As the aircraft Mach number increased, the spike translated rearward and the second cone expanded according to the preset control system schedule. In this way increased compression was obtained as the supersonic flow was decelerated by two conical shocks prior to deceleration to subsonic velocities through a normal shock near the cowl lip.

In addition to the automatic air-induction control system, the left-hand inlet of the test airplane was equipped with a manual inlet control package which enabled the pilot to override the automatic system and adjust the spike and second cone to any desired position.

Figures 4(a) and 4(b) show a front view of the inlet with the spike moved full forward and the second cone fully collapsed and fully expanded, respectively. Figures 4(c) and 4(d) show the spike moved full aft, again fully collapsed and fully expanded. Figures 4(a) to 4(d) show the blunt-lip cowl configuration, and figure 4(e) shows the sharp-lip cowl configuration. They also show the splitter plate, three subinlets,

some of the vortex generators, the boundary-layer bleed perforations, and the boundary-layer rakes. In addition, two of the three inlet control sensors are shown in figure 4(a), the local Mach sensor beneath the wing glove and the lip shock sensor inside the lip.

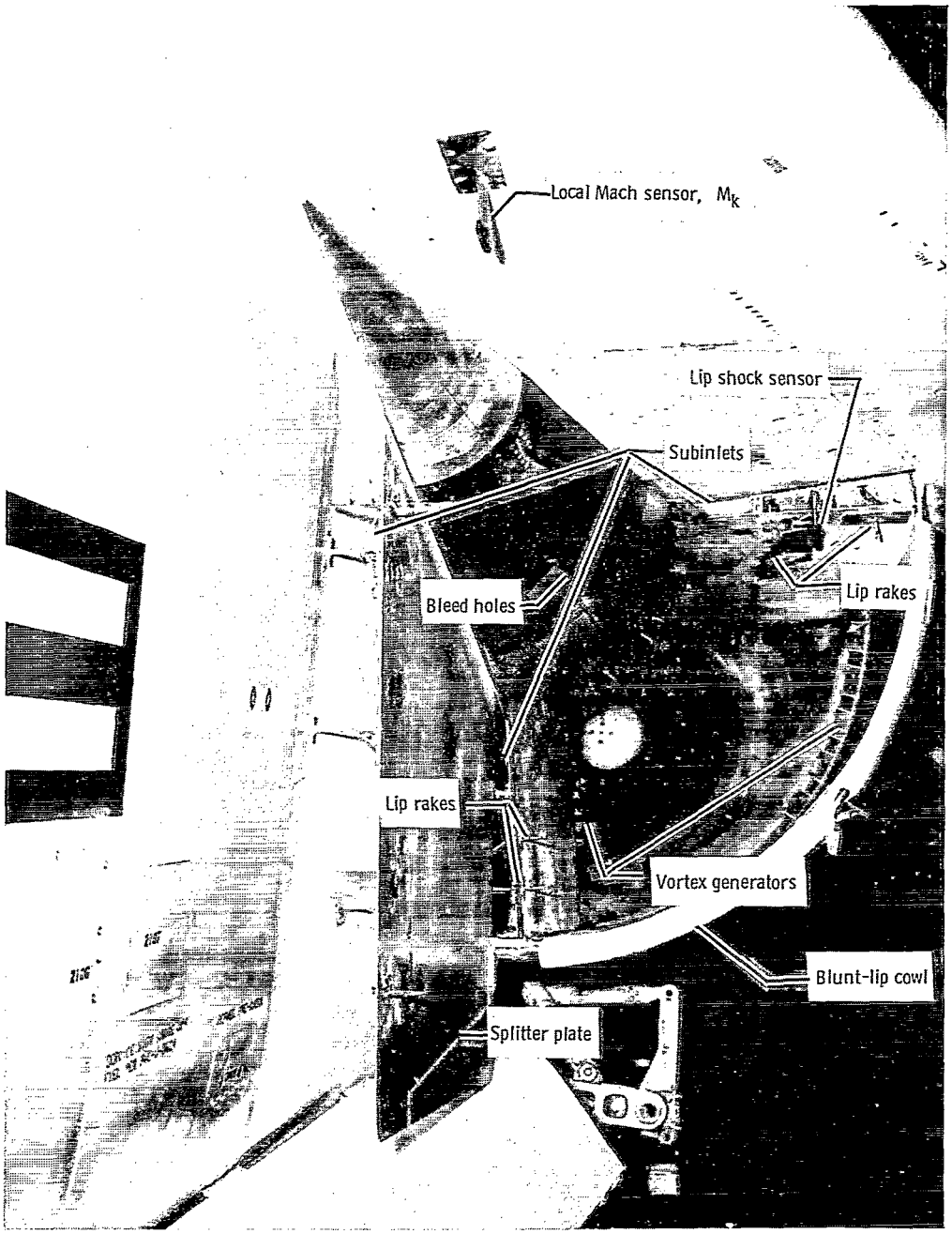

E-21372

(a) Spike full forward, $\frac{X}{R} = 2.24$*; second cone fully collapsed,* $\theta_{sca} = 10.8^{o}$*; blunt-lip cowl.*

Figure 4. F-111A airplane left inlet lip region.

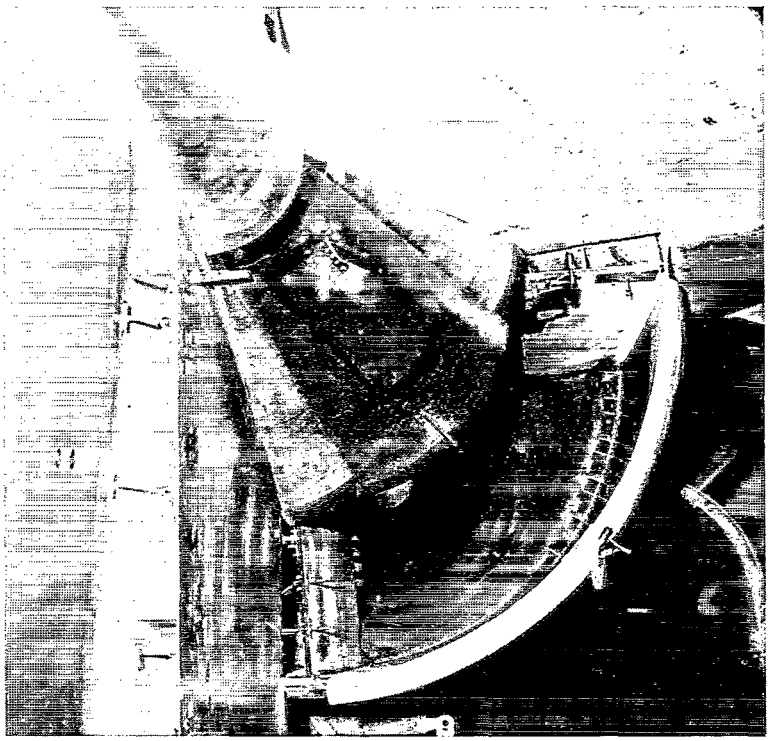

E-21382

(b) Spike full forward, $\frac{X}{R} = 2.24$; second cone fully expanded, $\theta_{sca} = 24.3^{o}$; blunt-lip cowl.

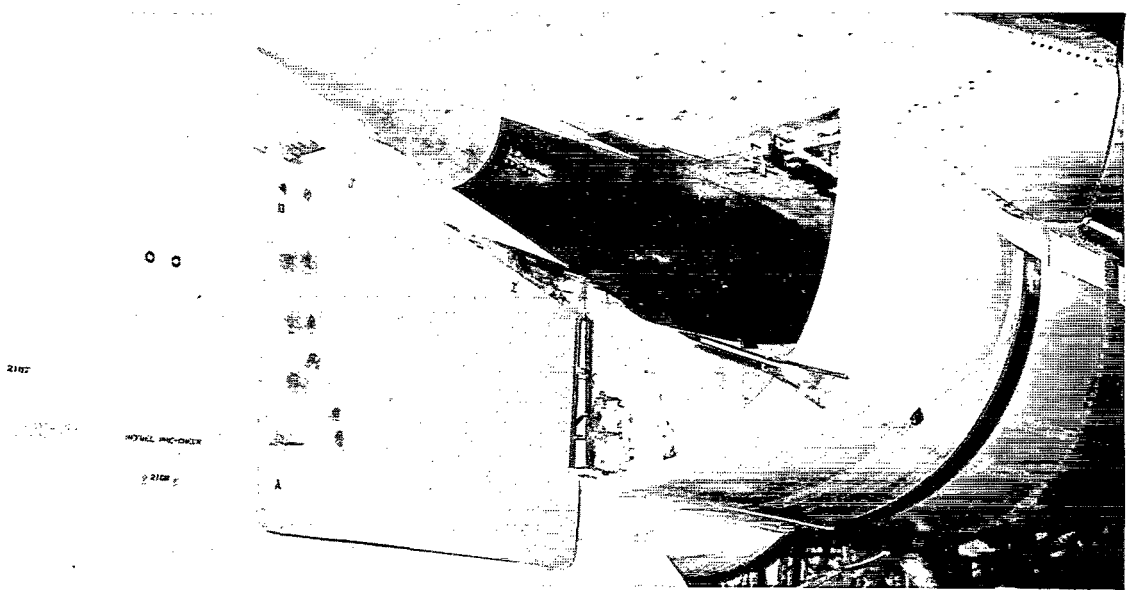

E-21376

(c) Spike full aft, $\frac{X}{R} = 1.65$; second cone fully collapsed, $\theta_{sca} = 10.8^{o}$; blunt-lip cowl.

Figure 4. Continued.

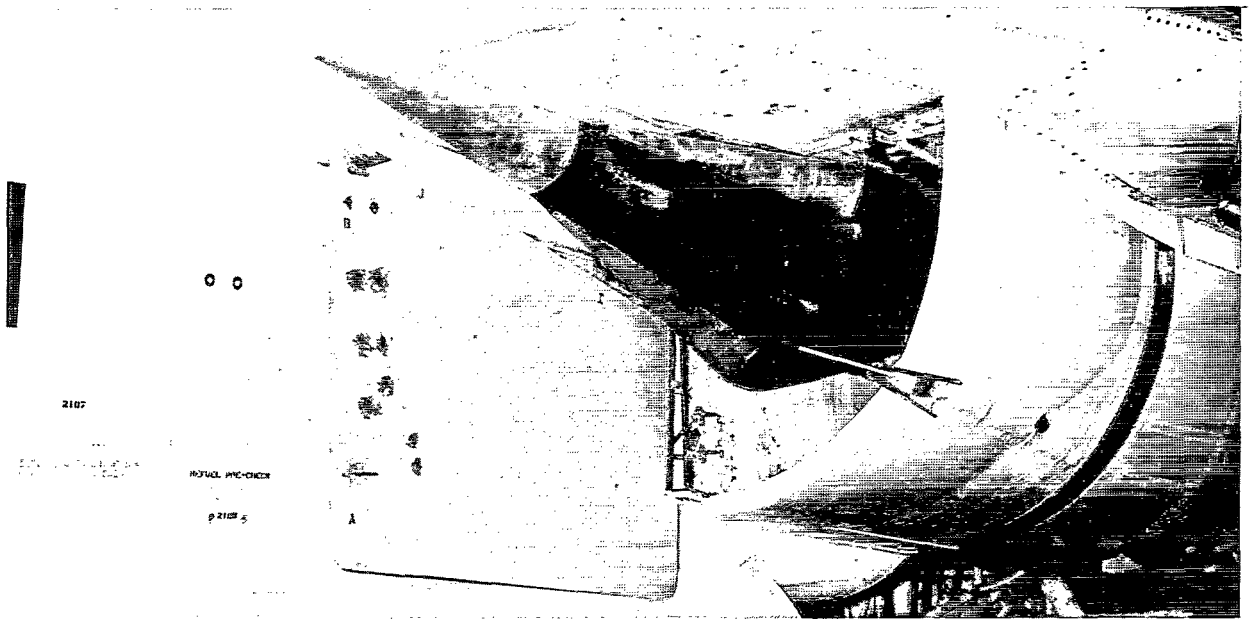

E-21377

(d) Spike full aft, $\frac{X}{R} = 1.65$; second cone fully expanded, $\theta_{sca} = 24.3^{o}$; blunt-lip cowl.

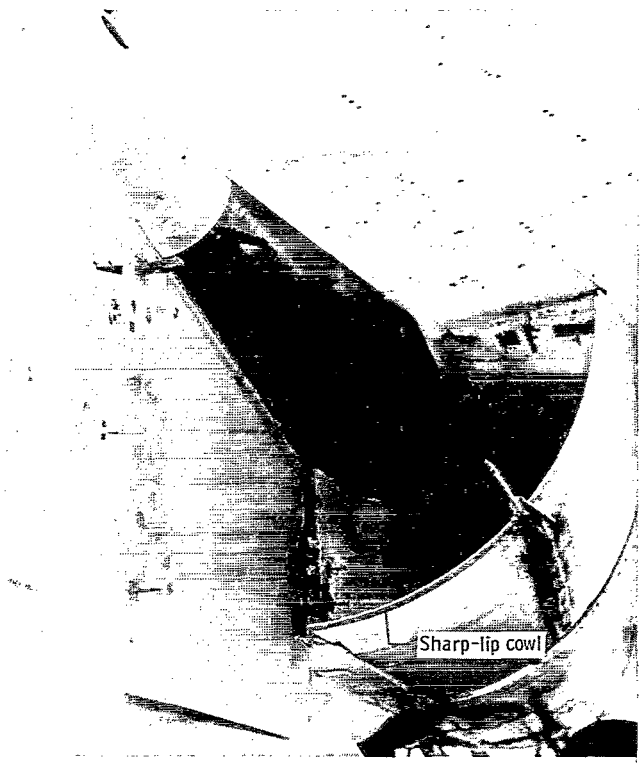

E-19106

(e) Sharp-lip cowl.

Figure 4. Concluded.

INSTRUMENTATION AND DATA ACQUISITION

The locations of the pressure sensors in the left inlet used to obtain data during these tests are shown in figure 5. Total-pressure measurements were obtained at the inlet lip from the outermost probes on boundary-layer rakes which were 4.45 centimeters (1.75 inches) from the surface. Also, low-response total-pressure measurements were obtained at the compressor face from probes on four equally spaced horizontal and vertical rakes. All probes were mounted at the centers of five equal annular flow areas in concentric circular arrangements called rings [1].

High-response (400 samples per second) static pressures were measured at various locations down the inlet duct from wall-mounted miniature transducers. High-response total pressures were obtained on the diagonal compressor face rakes from miniature transducers mounted within the rakes such that the distance from the probe tips to the transducer elements was less than 3.8 centimeters (1.5 inches). Before the transducers were installed in the test airplane, each probe-sensor configuration

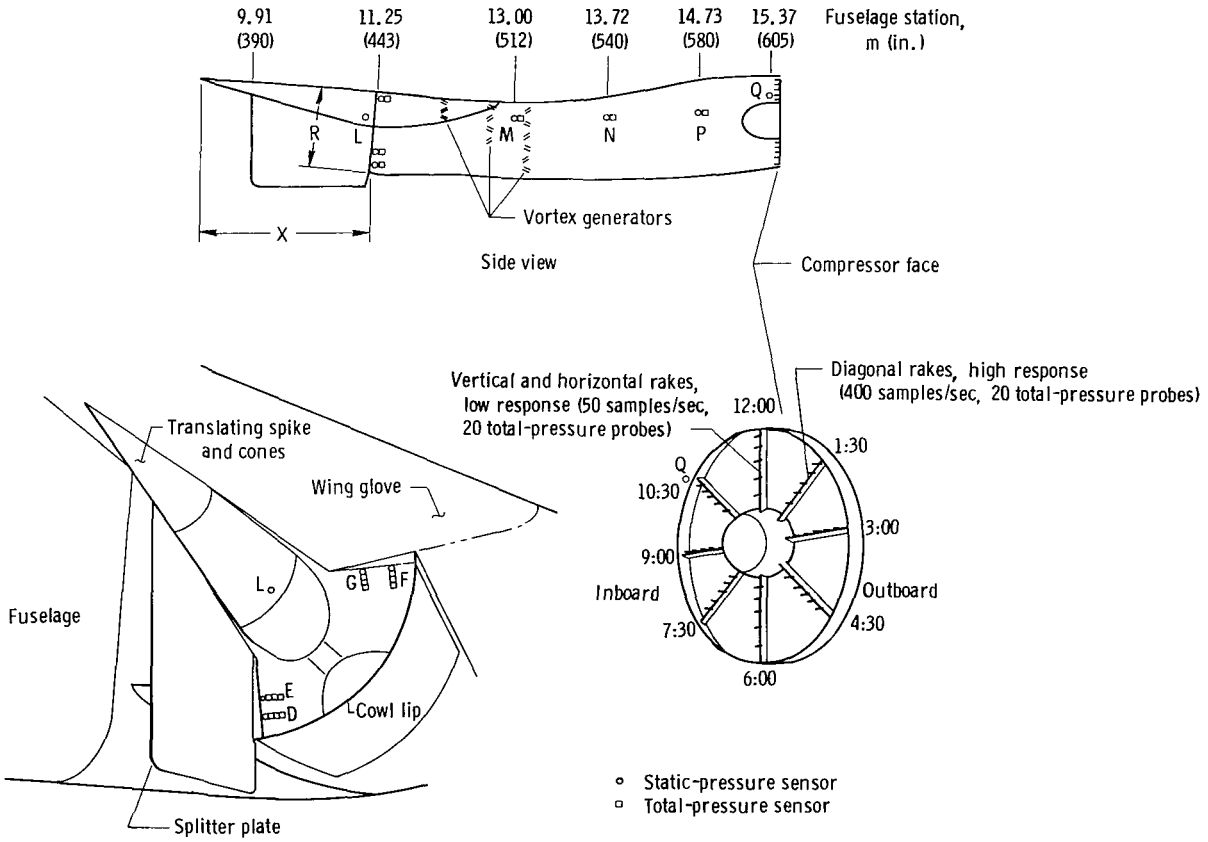

Figure 5. F-111A airplane left inlet duct and instrumentation.

[1] A ring is defined as a series of probes at constant radius from the engine centerline but at various circumferential positions.

was checked with sinusoidal oscillating pressures to insure a flat frequency response with no significant phase lag up to 200 hertz. Development of the high-response instrumentation is described in reference 1.

References 1 and 2 provide more detailed descriptions of the inlet and engine instrumentation. Reference 2 also describes the two 80-channel pulse code modulation systems used to record the test data.

PROCEDURE

Test Description

The data were recorded during 14 flights of the F-111A test airplane. They were obtained at Mach numbers from 0.68 to 2.18 and at altitudes of approximately 3050 meters (10,000 feet), 9150 meters (30,000 feet), and 13,700 meters (45,000 feet) with both blunt-lip and sharp-lip cowl configurations.

For a given test condition the airplane was first trimmed by the pilot for stabilized level flight with the engines at or in excess of military power. Angle of sideslip, β, was essentially zero for these data runs. Data were then recorded with the inlet geometry in the automatic position. Subsequently, the pilot switched over from automatic to manual control and proceeded to vary the spike position or second-cone angle as prearranged while holding the other variable constant. Small increments in either inlet variable were used in this way to obtain successive off-design performance data points and to thus isolate the effects of a particular variable. This procedure was continued until the spike was fully forward or aft, until the second cone was fully collapsed or expanded, or until a compressor stall occurred. If a compressor stall occurred, the pilot immediately switched back from manual to automatic inlet control and initiated engine recovery procedures.

Data Analysis

Computer programs were written to calculate the inlet performance parameters, total-pressure recovery, η, total-pressure distortion, D, total-pressure distortion factor, K_D, turbulence factor, Tu, for both total and static pressures, and mass-flow ratio, $\frac{w_2}{w_\infty}$. Equations defining these quantities are presented in appendix B.

PRECISION

The following table lists approximate maximum errors in important measured and derived quantities, taking into account repeatability:

Parameter	Maximum error
Free-stream Mach number, M_∞	±0.5 percent of value
Altitude, h	±33.5 m (±110 ft)
Angle of attack, α	±0.3°
Total temperature, T_t	±2.8° C (±5.0° F)
Spike position ratio, $\frac{X}{R}$	±1.0 percent of value
Second-cone angle, θ_{sca}	±0.5°
Airflow, w	±2.0 percent of value
Mass-flow ratio, $\frac{w_2}{w_\infty}$	±2.4 percent of value
Total pressure, p_t	±1.45 kN/m^2 (±0.21 lb/in.^{2})
Free-stream total pressure, $p_{t,\infty}$	±0.83 kN/m^2 (±0.12 lb/in.^{2})
Total-pressure recovery, η	±2.6 percent
Total-pressure distortion, D	±13 percent of value
Turbulence factor, Tu	±2.2 percent of value
Total-pressure distortion factor, K_D	±15 percent of value

RESULTS AND DISCUSSION

Inlet Performance During Automatic Operation

The flight-determined spike and second-cone-angle positions which resulted during automatic control of the test inlet over the Mach number range from 0.68 to 2.18 and at nominal altitudes of 3050 meters (10,000 feet), 9150 meters (30,000 feet), and 13,700 meters (45,000 feet) are summarized in figure 6. As shown, second-cone angle is a function of altitude as well as Mach number. For 13,700 meters (45,000 feet) altitude, the θ_{sca} data show approximately ±1.5° of scatter.

Figure 7(a) presents local Mach number, M_k, measured ahead of the test inlet at 13,700 meters (45,000 feet) altitude during stabilized flight at free-stream Mach numbers of 1.38 to 2.18 while the inlet was functioning automatically in accordance with the preset schedule. The scatter in these data is attributed largely to angle-of-attack effects in the M_k measurement discussed in reference 5 and shown in figure 7(b).

The curves of constant α shown in figure 7(b) were derived from data recorded during windup turns in which the pilot banked and increased normal acceleration while keeping engine settings fixed. Thus, for a given M_∞, increasing α results in decreasing M_k. It is apparent, then, that some variation in inlet geometry will result during a maneuver because of the effect of α on M_k, which is one of the inlet automatic controller inputs.

Figure 7(c) shows the approximate inlet throat Mach number, which was determined by assuming an idealized flow model based on the in-flight measurements of

M_k shown in figure 7(a) and θ_{sca} and then calculating Mach number M_1 (valid near the spike surface in an axial plane through the local Mach sensor position) through the three shock waves. Conical shock theory was assumed to apply through the first two shocks and normal shock theory through the discontinuity at the cowl lip (ref. 6).

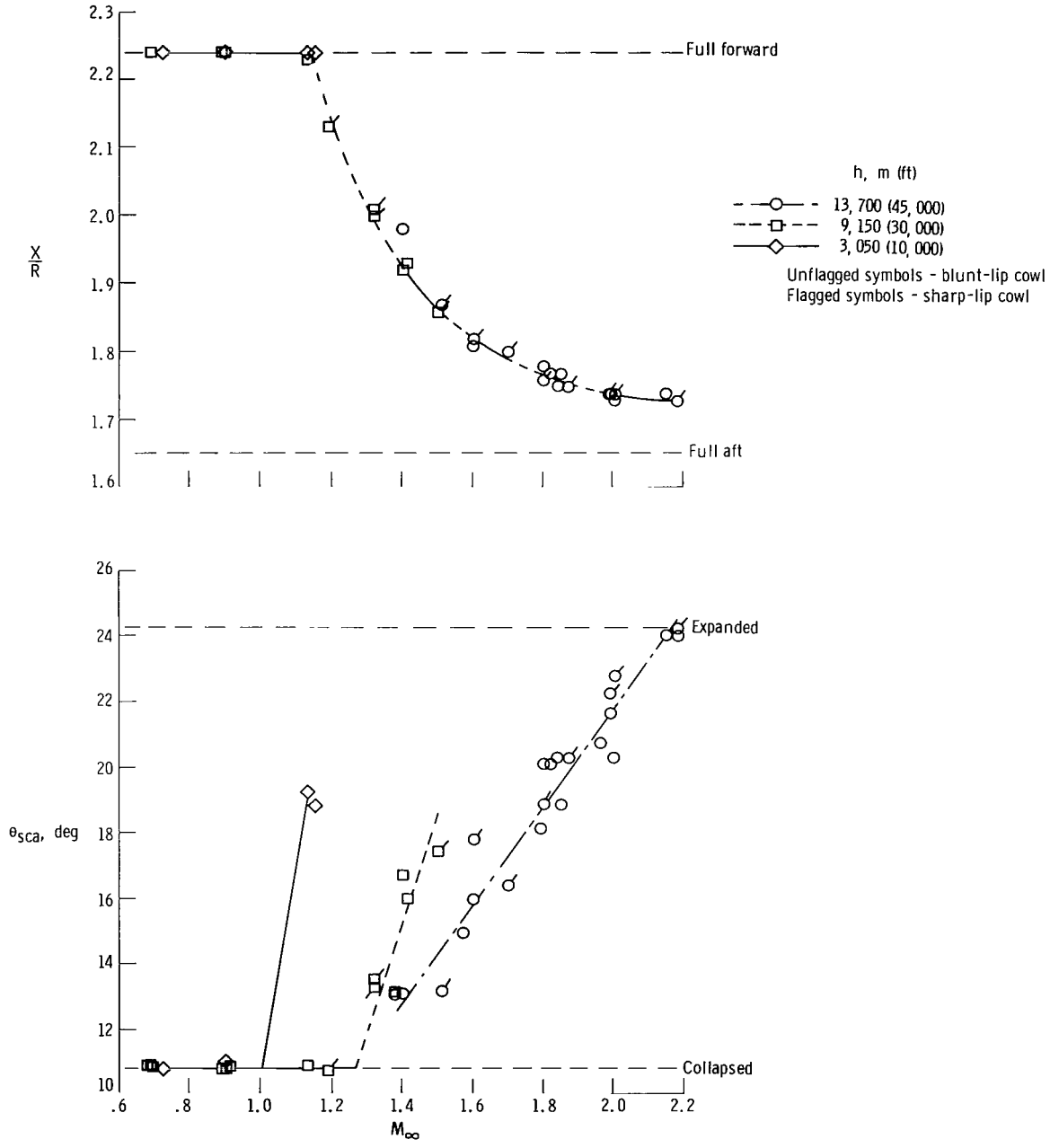

Figure 6. Scheduled spike position and second-cone angles obtained in flight.

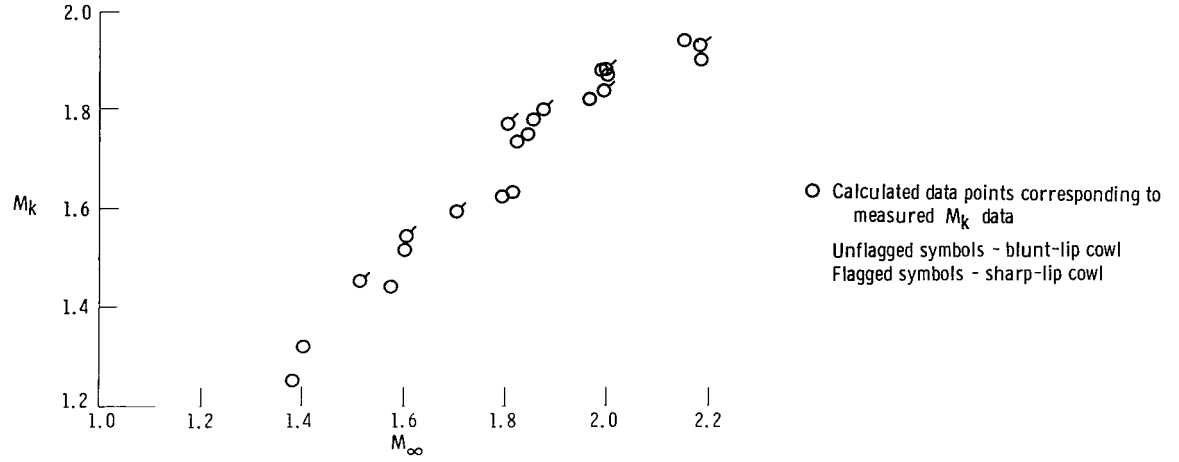

(a) Measured local Mach number ahead of the inlet.

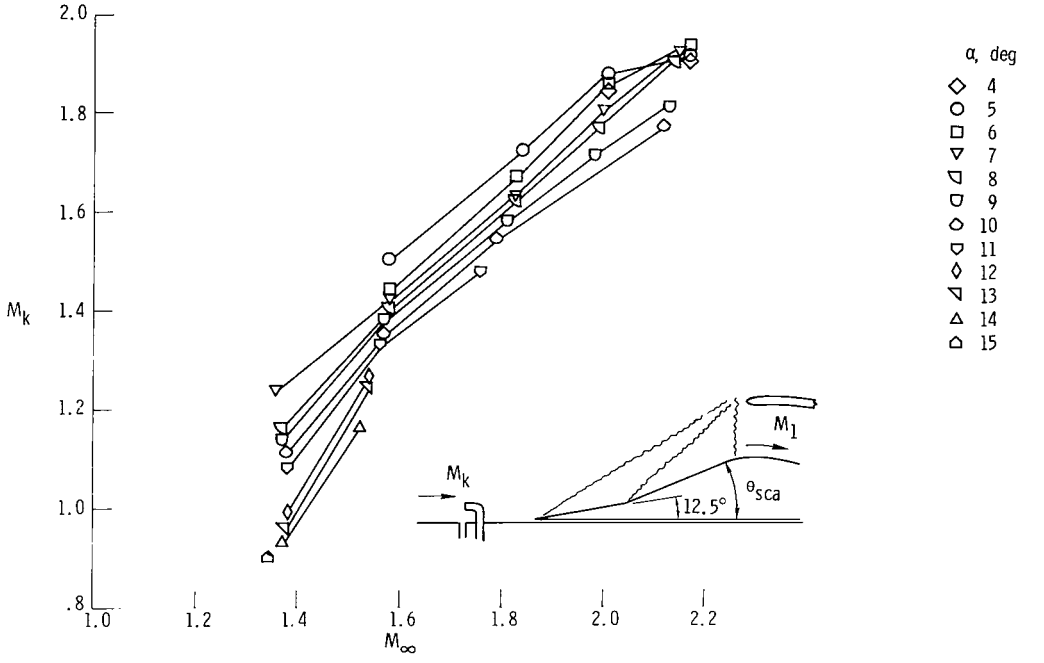

(b) Effect of α on M_k; flight data.

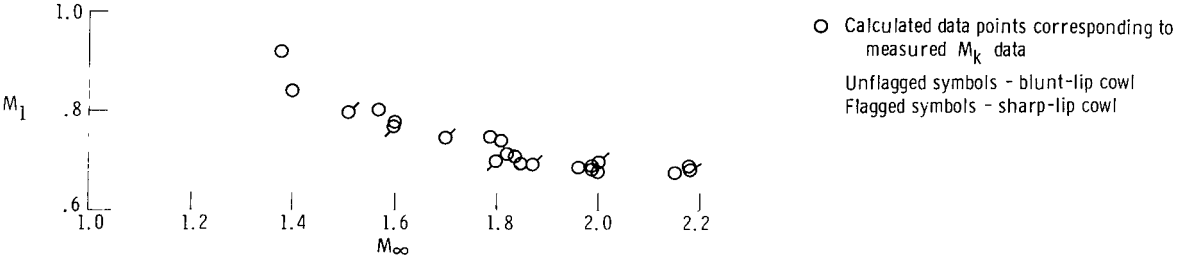

(c) Calculated Mach number aft of the normal shock.

Figure 7. Surface Mach numbers ahead of and near the spike at h = 13,700 meters (45,000 feet).

Total-pressure recovery, η_2, distortion, D, distortion factor, K_D, mass-flow ratio, $\frac{w_2}{w_\infty}$, and engine-corrected airflow, $w_{2,c}$ are plotted as functions of free-stream Mach number, M_∞, in figures 8(a) to 8(e), respectively. The data shown in these

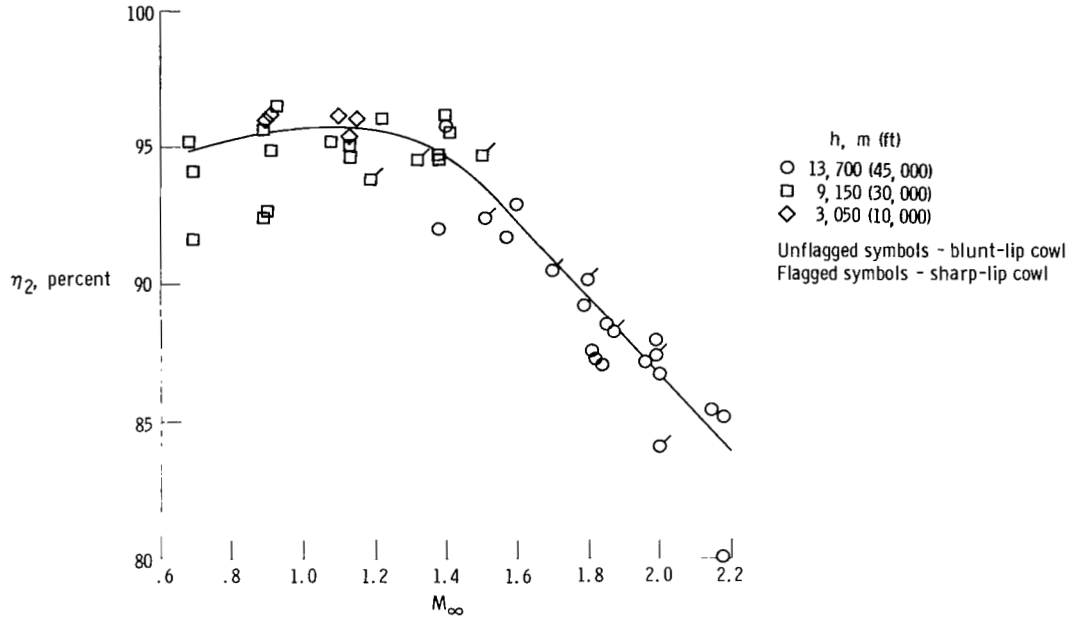

(a) Total-pressure recovery.

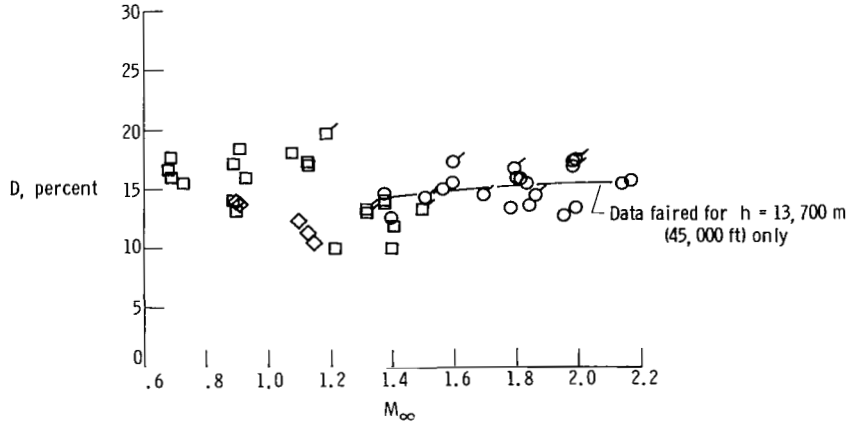

(b) Total-pressure distortion.

Figure 8. Inlet performance during automatic control with sharp- and blunt-lip cowls.

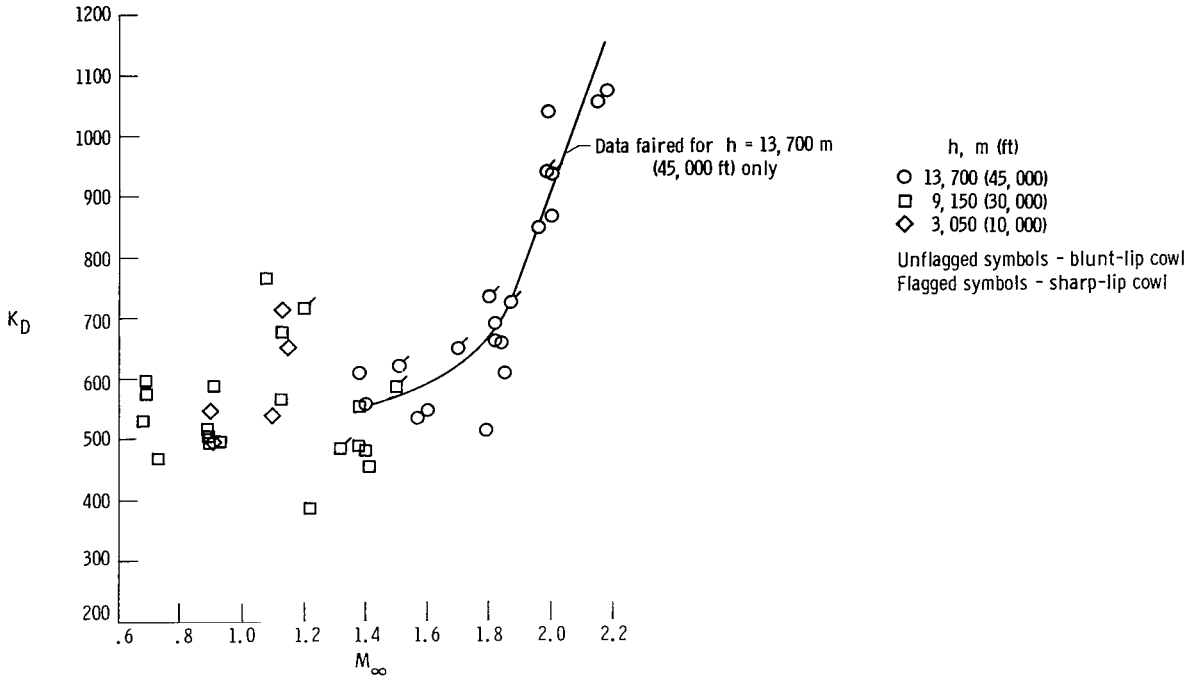

(c) Distortion factor.

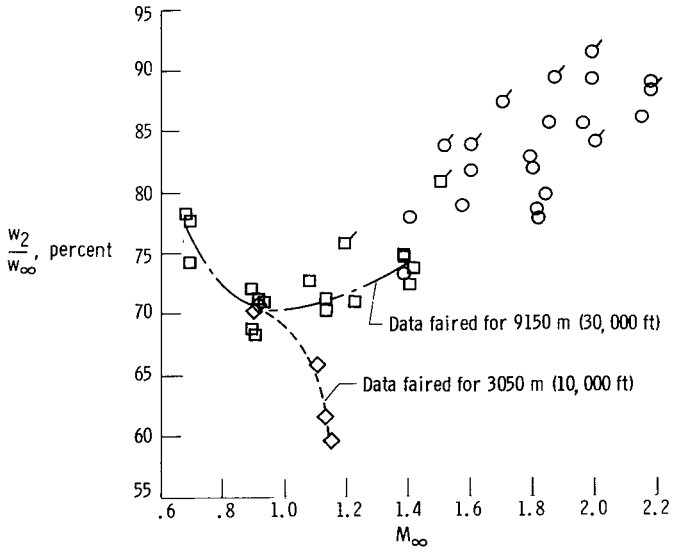

(d) Mass-flow ratio.

Figure 8. Continued.

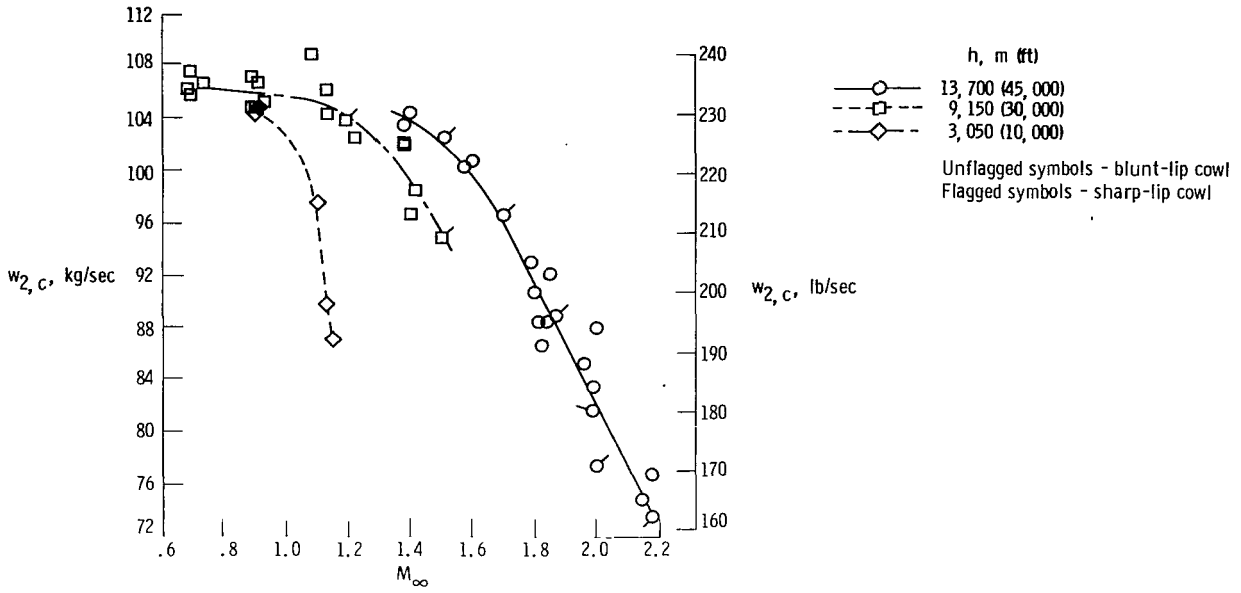

(e) Engine-corrected airflow.

Figure 8. Concluded.

figures were recorded during stabilized flight with automatic inlet operation at altitudes of 3050 meters (10,000 feet), 9150 meters (30,000 feet), and 13,700 meters (45,000 feet). An attempt was made to fair smooth curves where possible. It is evident from these figures that a relatively wide range in the inlet performance parameters, η_2, D, K_D, and $\frac{w_2}{w_\infty}$, may be expected during normal operation of an inlet of this type. The data scatter is attributed largely to differences in mass-flow ratio for the points shown. Mass-flow ratio is shown to have a significant effect on η_2 and D in references 7 and 8.

The faired curve of measured total-pressure recovery from figure 8(a) is replotted in figure 9 for comparison with the design standard specified in MIL-E-5008C and the normal shock loss curve obtained from reference 6. The flight data have about a 3 percent lower recovery than the Military Specification data at Mach 1.4 and about a 6.5 percent lower recovery at Mach 2.2. The differences are attributed largely to energy losses inside the inlet, as discussed in the following paragraphs.

For the flow model associated with figure 7, total-pressure recovery behind the normal shock may be calculated by accounting for total-pressure losses through the three shock waves. In this procedure the local Mach number and second-cone angle obtained at each flight Mach number are used to calculate the total-pressure ratios from the conical wave curves and the normal shock tables of reference 6. The results of this simple computation for automatic schedule data at 13,700 meters

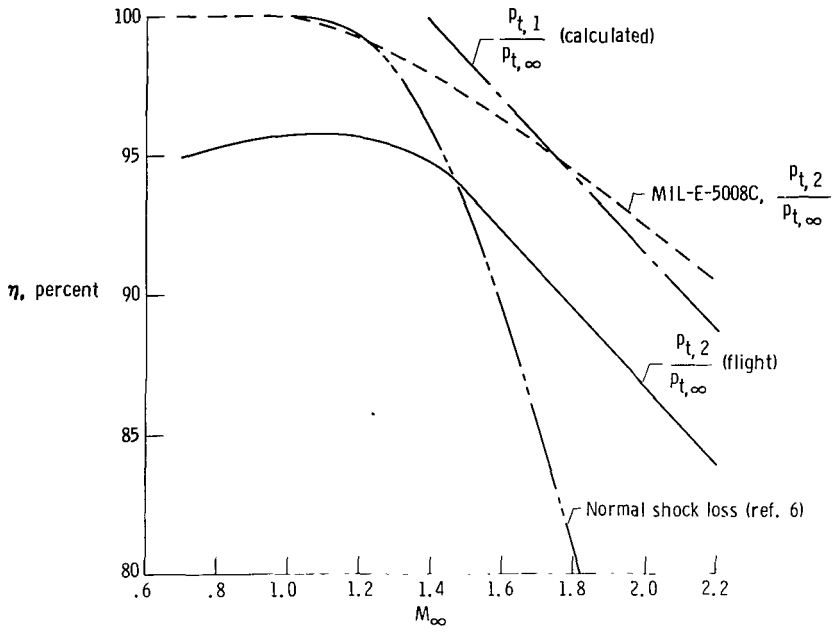

Figure 9. Comparison of faired compressor face total-pressure recovery, design standard inlet recovery, calculated recovery aft of the normal shock, and normal shock loss.

(45,000 feet) altitude are compared with mean compressor-face recovery in figure 9. From this figure, it appears that the air suffers somewhat uniform losses, about 5 percent inside the inlet independent of free-stream Mach number.

The calculated pressure recovery behind the normal shock near the spike surface and measured mean recovery at the compressor face for $M_\infty = 1.38$ to 2.18 from figure 9 are replotted in figures 10(a) to 10(d) for comparison with lip rake (outer probes) data for the same points. Most data meet or exceed the theoretical surface values. The most obvious exceptions are the data of rake E for all Mach numbers and of rake D for Mach numbers greater than 1.9.

The scatter in the data of figure 10 appears to be greater for probes D and E, on the fuselage side of the inlet, than for probes F and G, under the wing glove, probably because the low-energy boundary-layer air which had built up under the wing glove was more successfully removed than the air along the fuselage forebody and on the splitter plate. It is interesting to compare the scatter at probe D with that at probe E and the scatter at probe F with that at probe G. As noted previously, as the second cone expands with increasing M_∞ (fig. 6), the spike surface moves closer to the lip probes (fig. 4(b)). Apparently, the closer the spike surface is to the lip probes, the greater the scatter becomes. Also, of the pairs D and E and F and G, the probes nearer the spike surface show the greater scatter, possibly because of the presence of boundary layer air on the spike surface. Figures 10(c) and 10(d) show that the airflow passing rakes F and G had lower total-pressure losses, probably due to the favorable compression effects on the lower surface of the wing glove and an effective glove bleed.

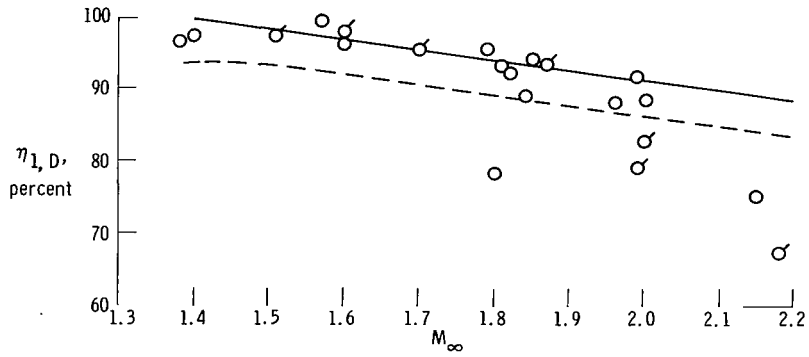

(a) Recovery measured at lip rake D.

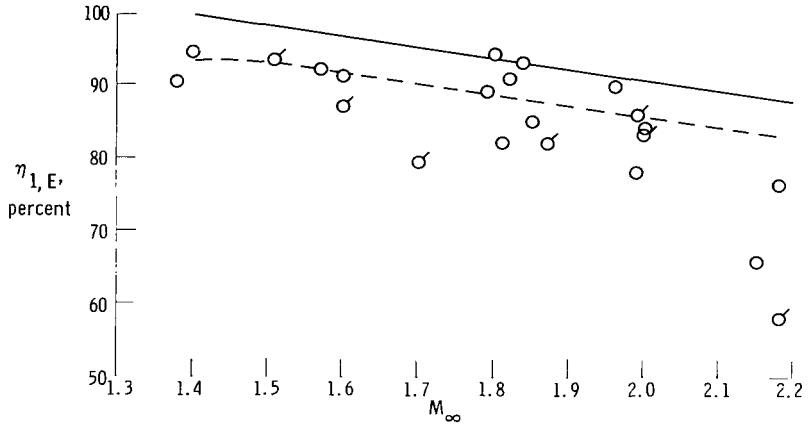

(b) Recovery measured at lip rake E.

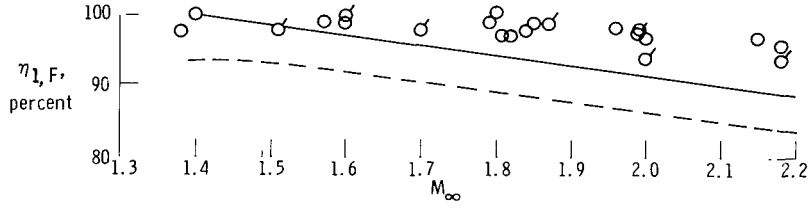

(c) Recovery measured at lip rake F.

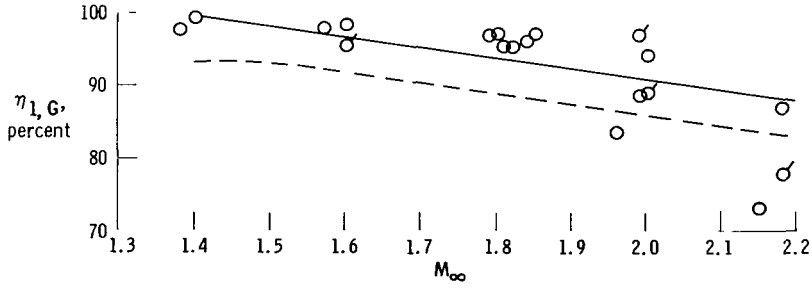

(d) Recovery measured at lip rake G.

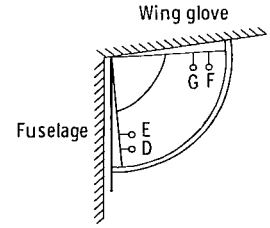

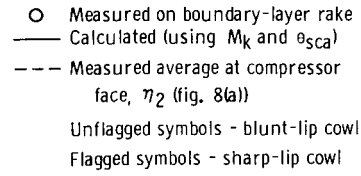

Figure 10. Comparison of calculated total-pressure recovery behind the normal shock, measured average total-pressure recovery at the compressor face, and total-pressure recovery measured by the boundary-layer lip rakes at h = 13,700 meters (45,000 feet).

Inlet Performance During Off-Schedule Operation

During numerous flight tests of the F-111A airplane, the pilot manually offset the spike and second-cone angle from the automatically scheduled positions. Figures 11 to 17 present data at Mach numbers and altitudes which typify off-schedule inlet performance over the flight-test range. The data presented in figures 11 to 15 were obtained with the blunt-lip cowl and those in figure 16 with the sharp-lip cowl.

Figures 11(a) and 11(b) show inlet performance during off-design movement of the spike and second-cone angle, respectively, at a Mach number of 0.7, an altitude of 9150 meters (30,000 feet), and an angle of attack of 6°. These figures illustrate the extreme sensitivity of mass-flow ratio, turbulence factor, the distortion factors, and total-pressure recovery to inlet geometry changes observed consistently during this type of test. The automatic points in both instances correspond to spike full

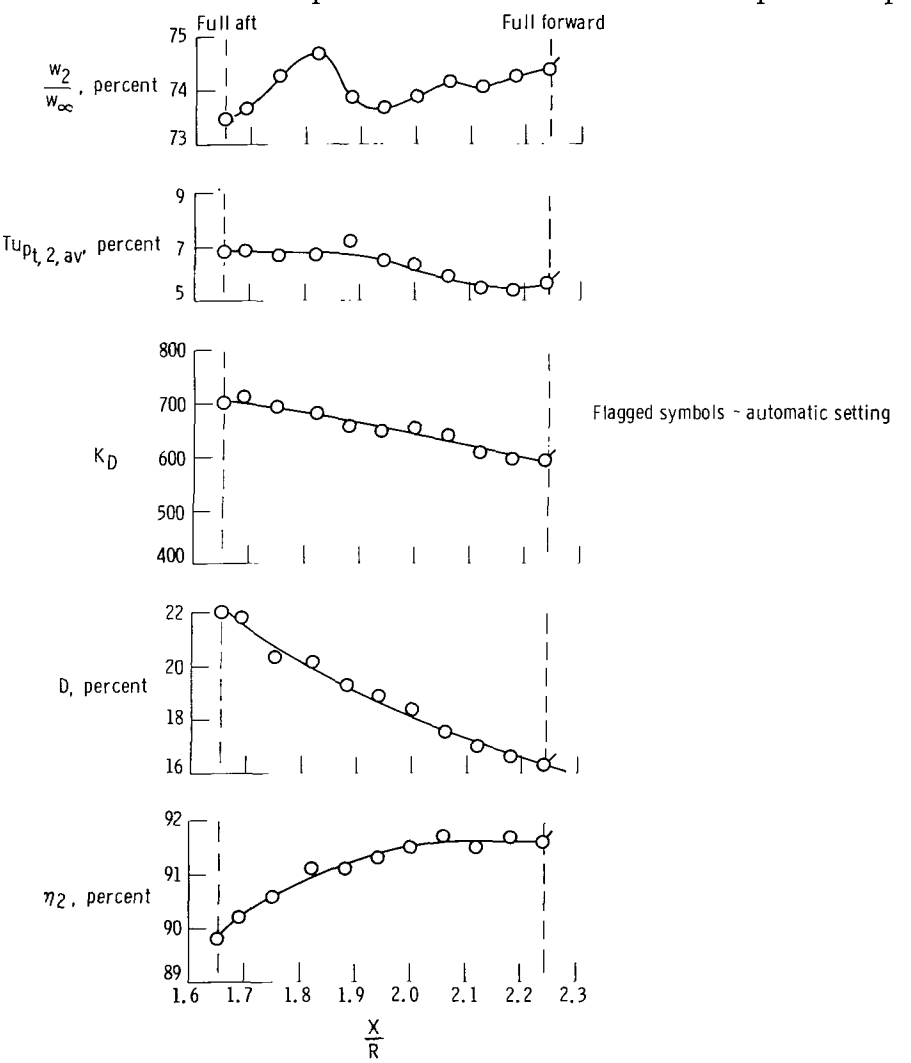

(a) Effect of manual spike movement with cone fully collapsed.

Figure 11. Effect of spike position and second-cone angle on inlet performance with blunt-lip cowl configuration at $\alpha = 6^o$, $M_\infty = 0.7$, and $h = 9150$ meters (30,000 feet).

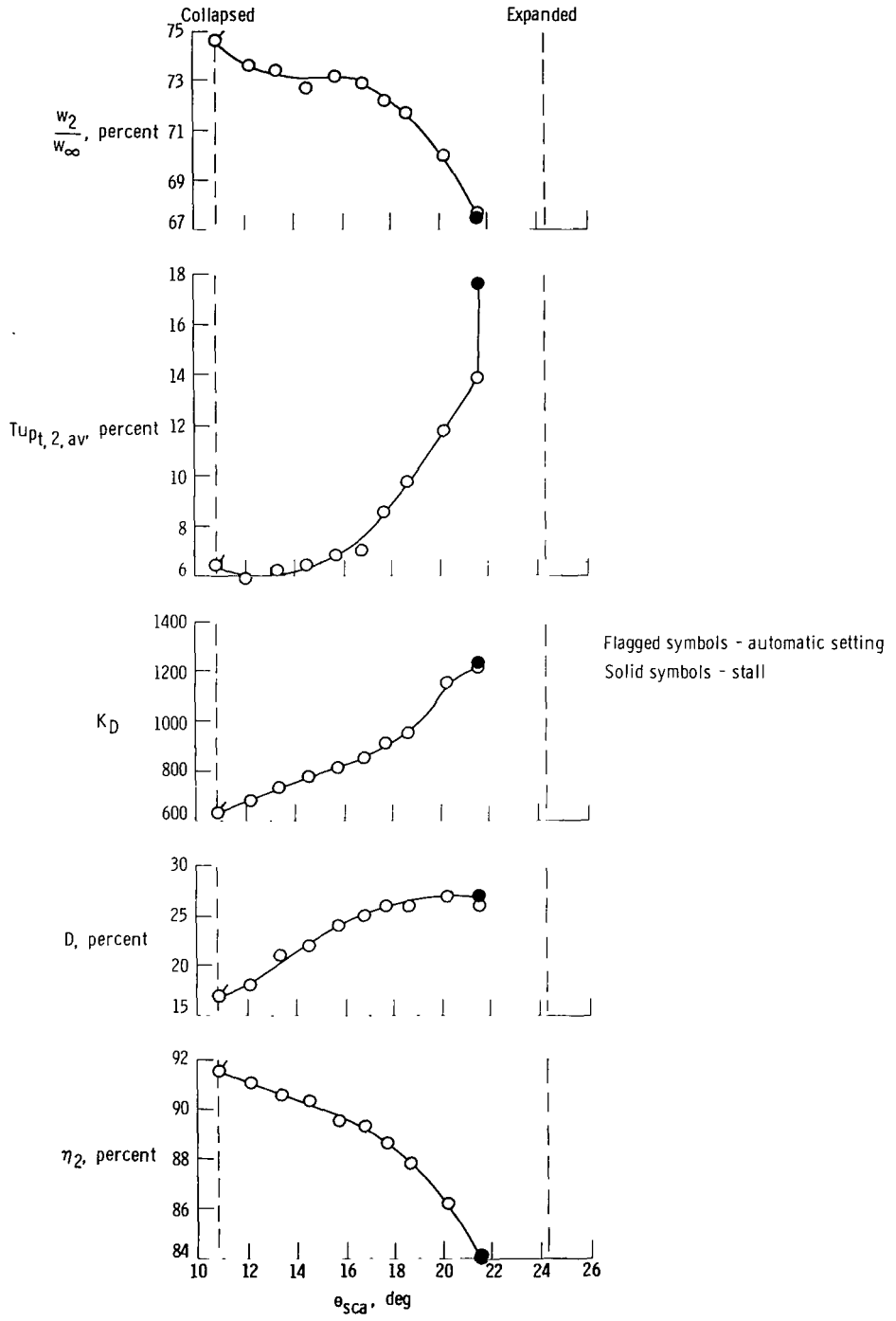

(b) Effect of manual second-cone-angle expansion with spike full forward.

Figure 11. Concluded.

forward $\left(\frac{X}{R} = 2.24\right)$ and cone fully collapsed $\left(\theta_{sca} = 10.8°\right)$. This condition was shown in figure 4(a). However, in figure 11(a) the spike was drawn fully to the rear with the cone held collapsed, which produced a gradual loss in performance. In figure 11(b) as the cone was expanded, with the spike held full forward, the flow distortion became so severe that a compressor stall occurred at $\theta_{sca} = 21.5°$ before the cone could be fully expanded to $\theta_{sca} = 24.3°$. Figure 4(b) shows the spike shape for full second-cone expansion.

The second-cone movement of figure 11(b), which resulted in a reduction of geometric throat area by approximately 11 percent, was characterized by a loss in η_2 from 91.5 percent to 84 percent. In addition, D increased from 17 percent to 27 percent, K_D increased 600 units, $Tu_{p_{t,2,av}}$ increased from 6 percent to 17.7 percent, and $\frac{w_2}{w_\infty}$ decreased from 74.7 percent to 67.6 percent.

Figures 12(a) and 12(b) show similar data from tests made at $M_\infty = 0.9$,

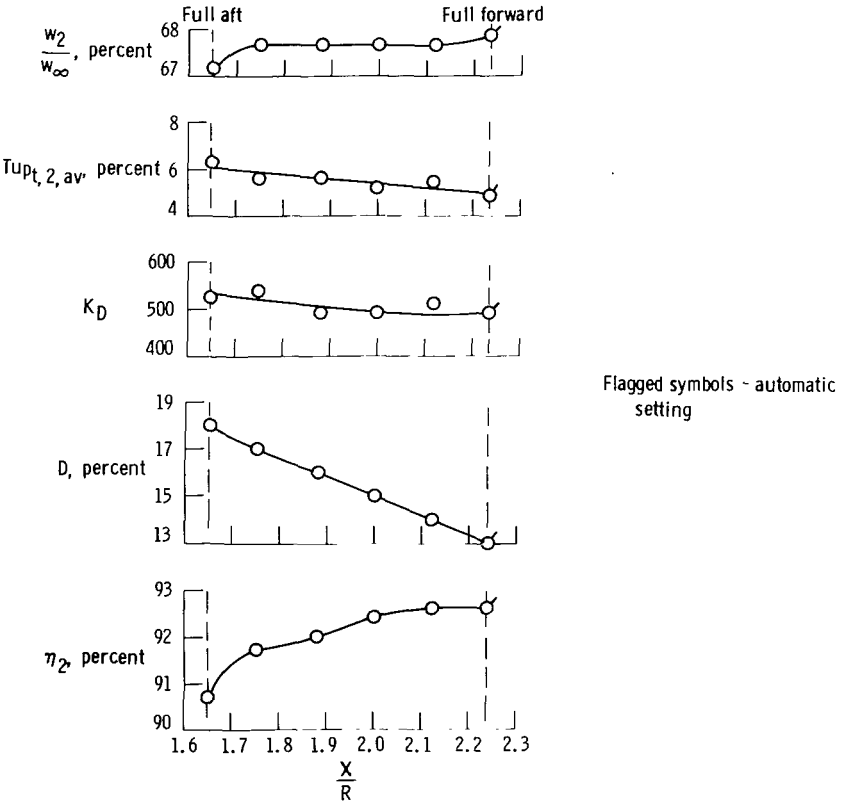

(a) Effect of manual spike movement with cone fully collapsed.

Figure 12. Effect of spike position and second-cone angle on inlet performance with blunt-lip cowl configuration at $\alpha = 5^o$, $M_\infty = 0.9$, and $h = 9150$ meters (30,000 feet).

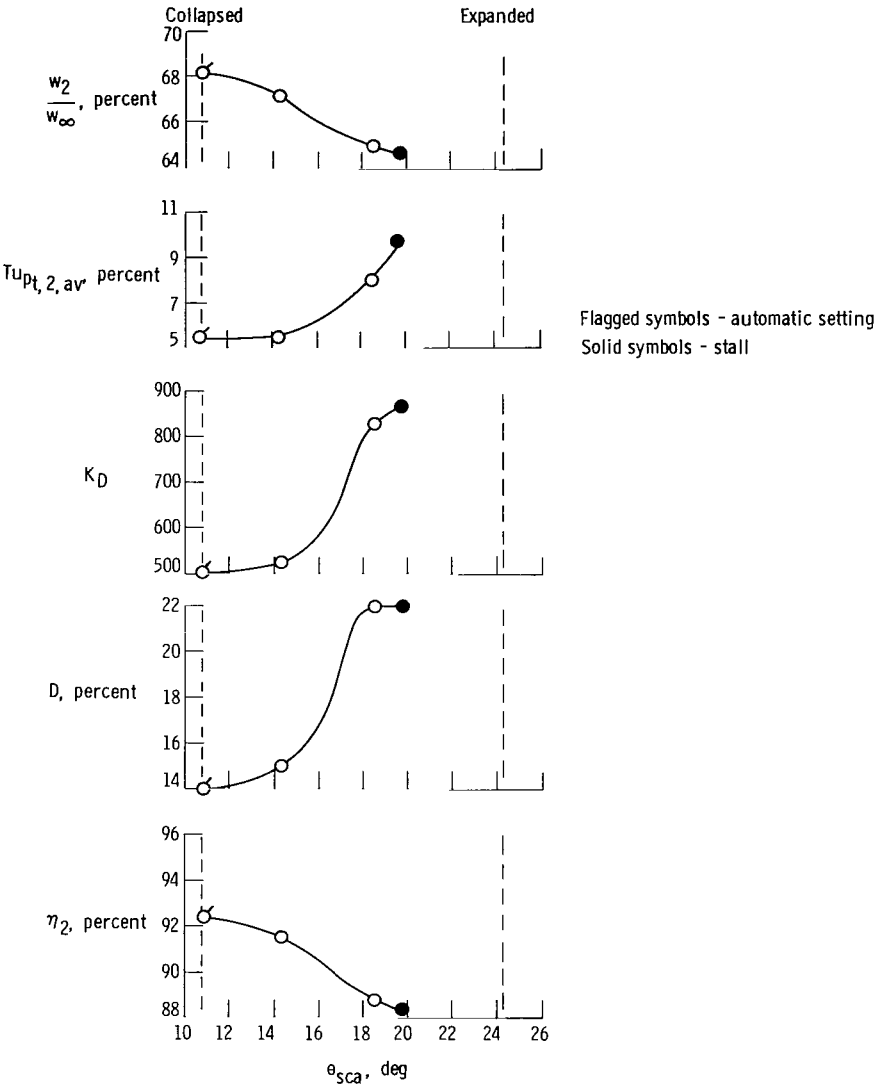

(b) Effect of manual second-cone-angle expansion with spike full forward.

Figure 12. Concluded.

h = 9150 meters (30,000 feet), and $\alpha = 5°$. As before, the off-schedule second-cone motion induced a compressor stall after a reduction in geometric throat area of about 8 percent and a loss in η_2 from 92.6 percent to 88.4 percent. Also, D increased from 14 percent to 22 percent, K_D increased 360 units, $Tu_{p_{t,2,av}}$ increased from 5.5 percent to 9.7 percent, and $\frac{w_2}{w_\infty}$ decreased from 68.2 percent to 64.7 percent. In general, this figure and figure 11 show that inlet performance was more sensitive

to second-cone expansion than to rearward spike movement in terms of adverse changes in the performance parameters.

Off-schedule data at $M_\infty = 1.4$, $h = 9150$ meters (30,000 feet), and $\alpha = 3°$ are presented in figures 13(a) and 13(b). The values of $\frac{X}{R}$ and θ_{sca} at the automatic point are consistent with those in figure 6. In this instance, wide excursions in inlet variables from the automatic settings were clearly detrimental, except for the rearward spike motion in figure 13(a) which produced little change in η_2, no change in D, and a small, favorable reduction in K_D.

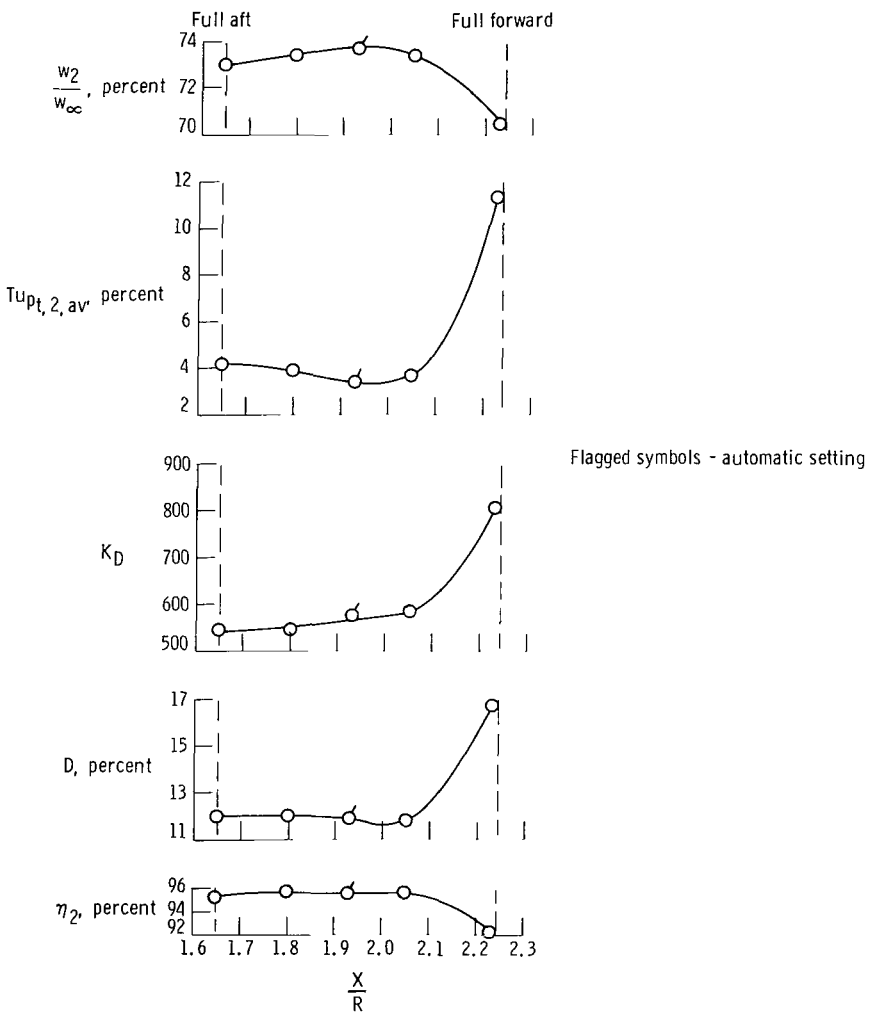

(a) Effect of manual spike movement with fixed second-cone angle, $\theta_{sca} = 16.1^O$.

Figure 13. Effect of spike position and second-cone angle on inlet performance with blunt-lip cowl configuration at $\alpha = 3^O$, $M_\infty = 1.4$, and $h = 9150$ meters (30,000 feet).

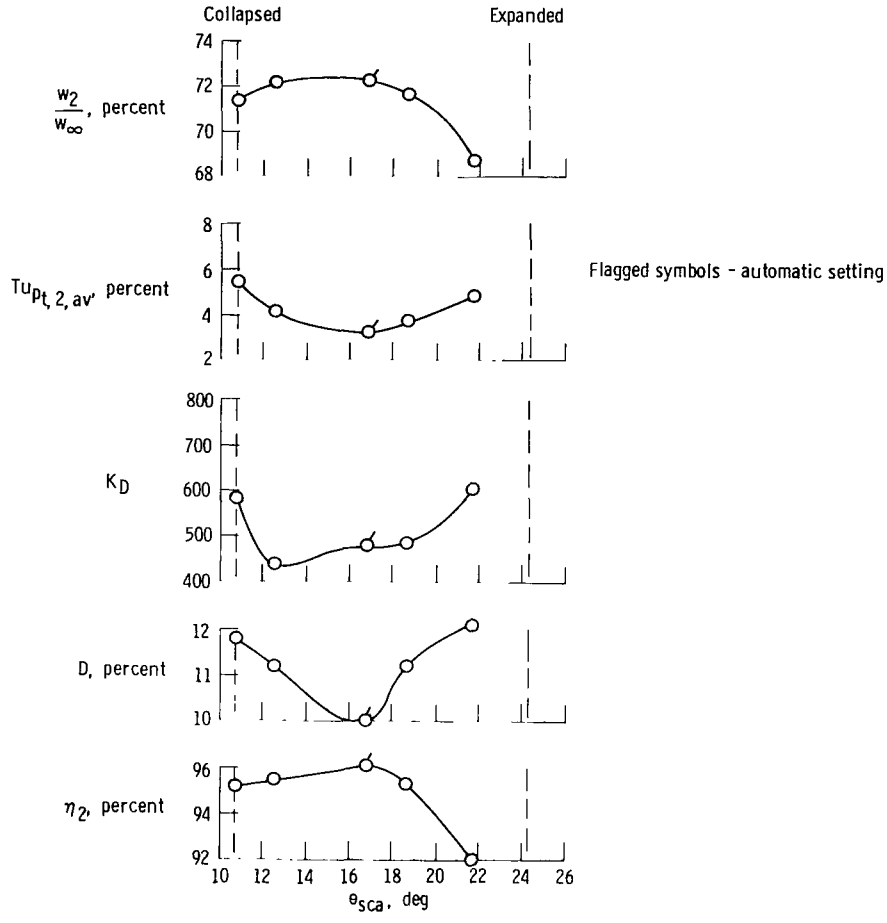

(b) Effect of manual second-cone-angle variation with spike position fixed at $\frac{X}{R} = 1.94$.

Figure 13. Concluded.

Figures 14(a) and 14(b) summarize results at $M_\infty = 1.6$, $\alpha = 5°$, and $h = 13,700$ meters (45,000 feet). Here, as in the previous figure, the rearward spike motion was least detrimental in terms of the performance parameters, although stalls were induced by advancing the spike and expanding the second cone.

Performance data at $M_\infty = 2.0$, $\alpha = 4°$, and $h = 13,700$ meters (45,000 feet) are presented in figures 15(a) and 15(b). Stalls resulted from relatively small forward spike motion and second-cone-angle reduction.

It is evident from figures 13 to 15 that inlet performance was most severely degraded by second-cone expansion but least severely by rearward spike movement. Some insight into the aspects of the flow field which were changing during spike and second-cone movements may be gained by noting that changes in θ_{sca} varied the strength of the second conical shock wave and consequently the flow entering the normal shock, whereas forward and rearward movements of the spike simply translated the conical shock waves. Thus, it might be expected that θ_{sca} would have

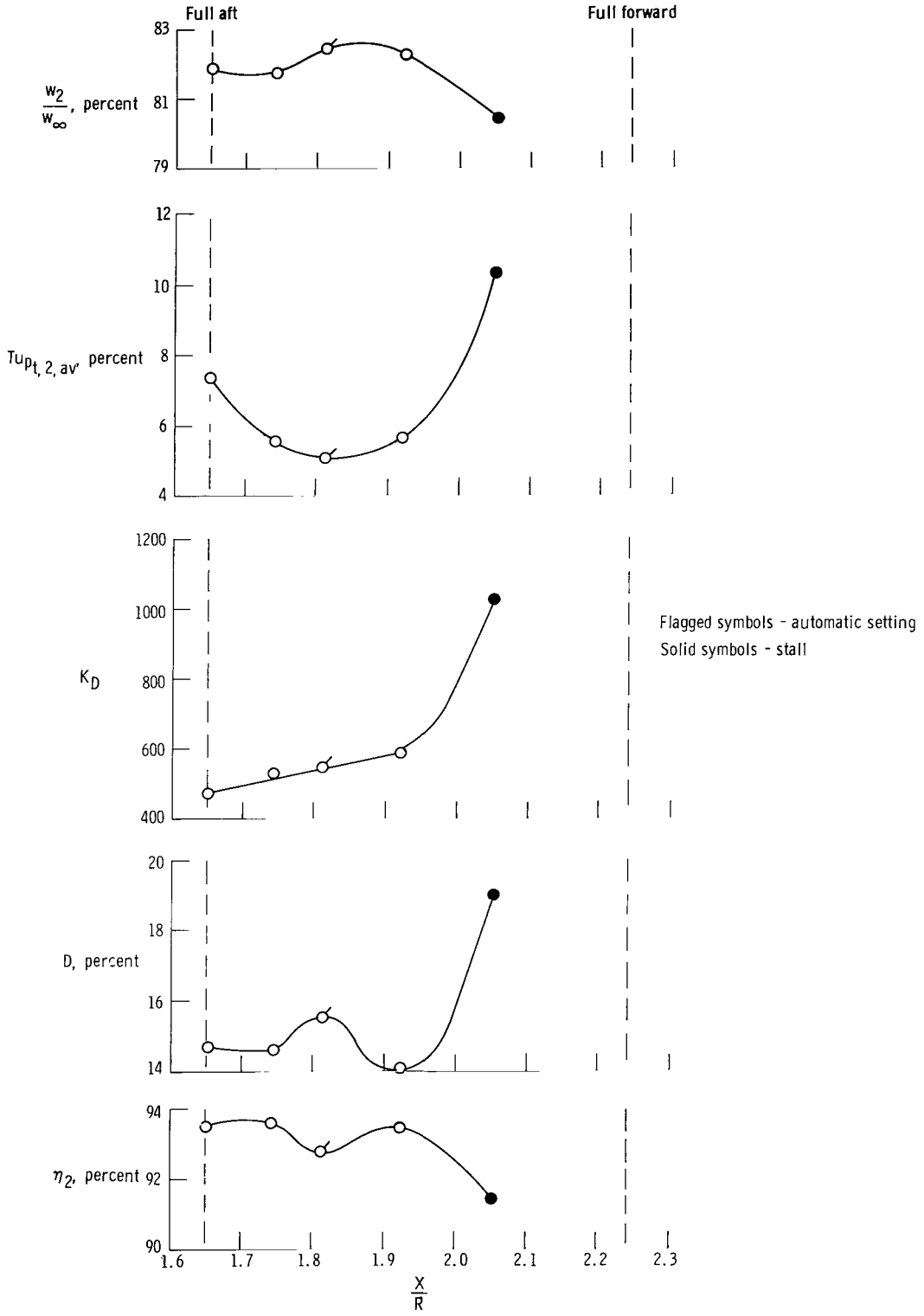

(a) Effect of manual spike movement with fixed second-cone angle, $\theta_{sca} = 16^o$.

Figure 14. Effect of spike position and second-cone angle on inlet performance with blunt-lip cowl configuration at $\alpha = 5^o$, $M_\infty = 1.6$, and $h = 13,700$ meters (45,000 feet).

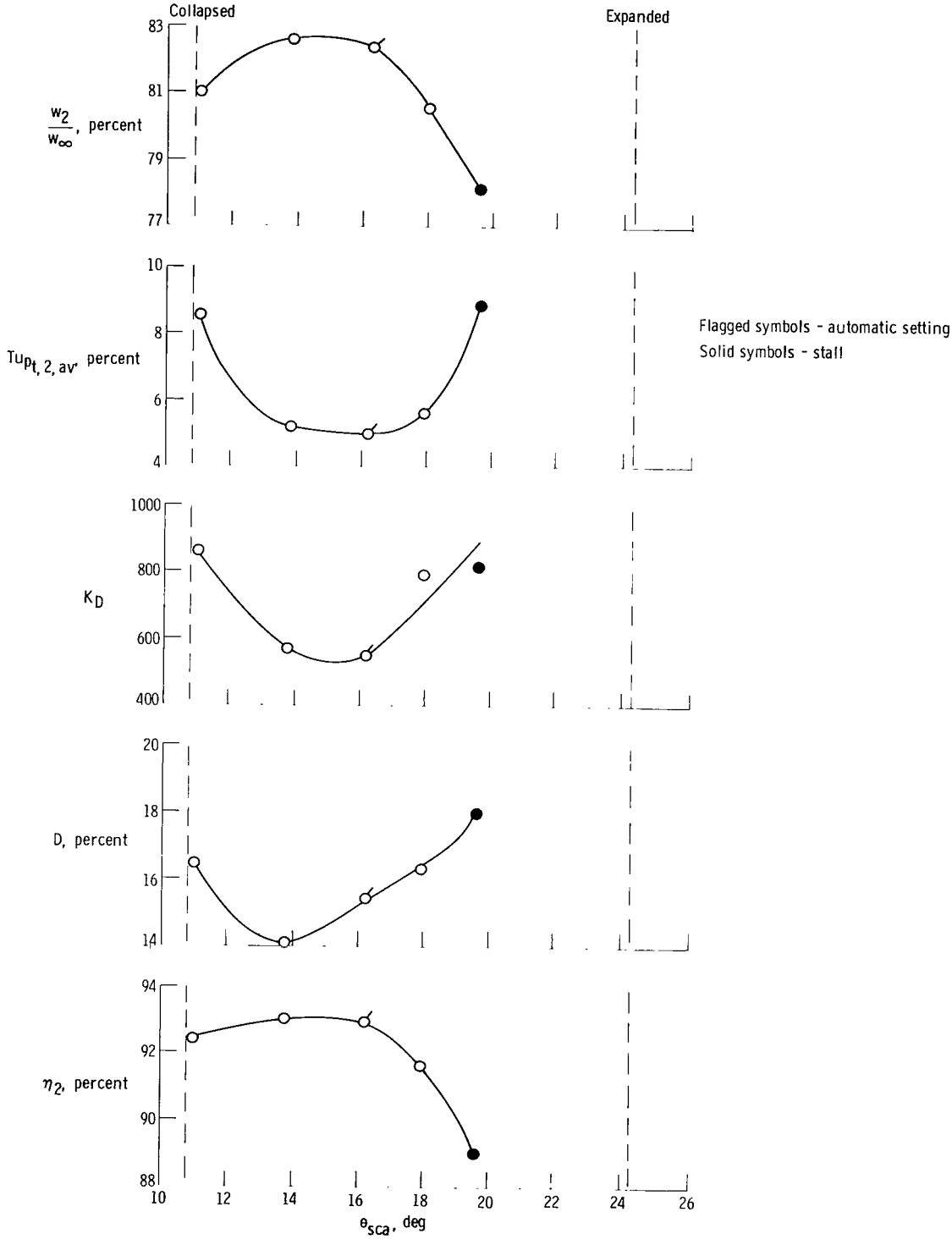

(b) Effect of manual second-cone-angle variation with spike fixed at $\frac{X}{R} = 1.82$.

Figure 14. Concluded.

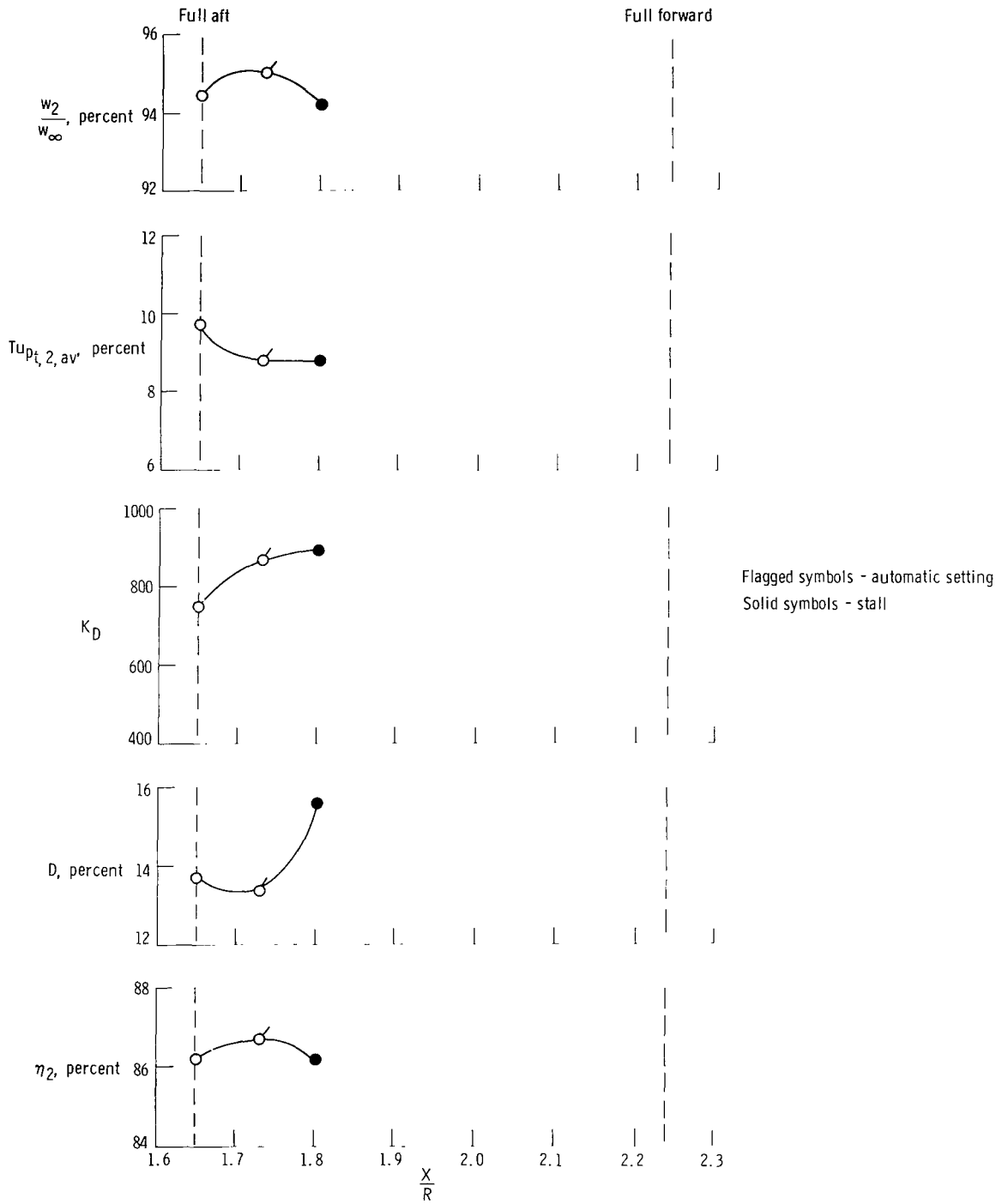

(a) Effect of manual spike movement with fixed second-cone angle, $\theta_{sca} = 20.6^{o}$.

Figure 15. Effect of spike position and second-cone angle on inlet performance with blunt-lip cowl configuration at $\alpha = 4^{o}$, $M_\infty = 2.0$, and $h = 13,700$ meters (45,000 feet).

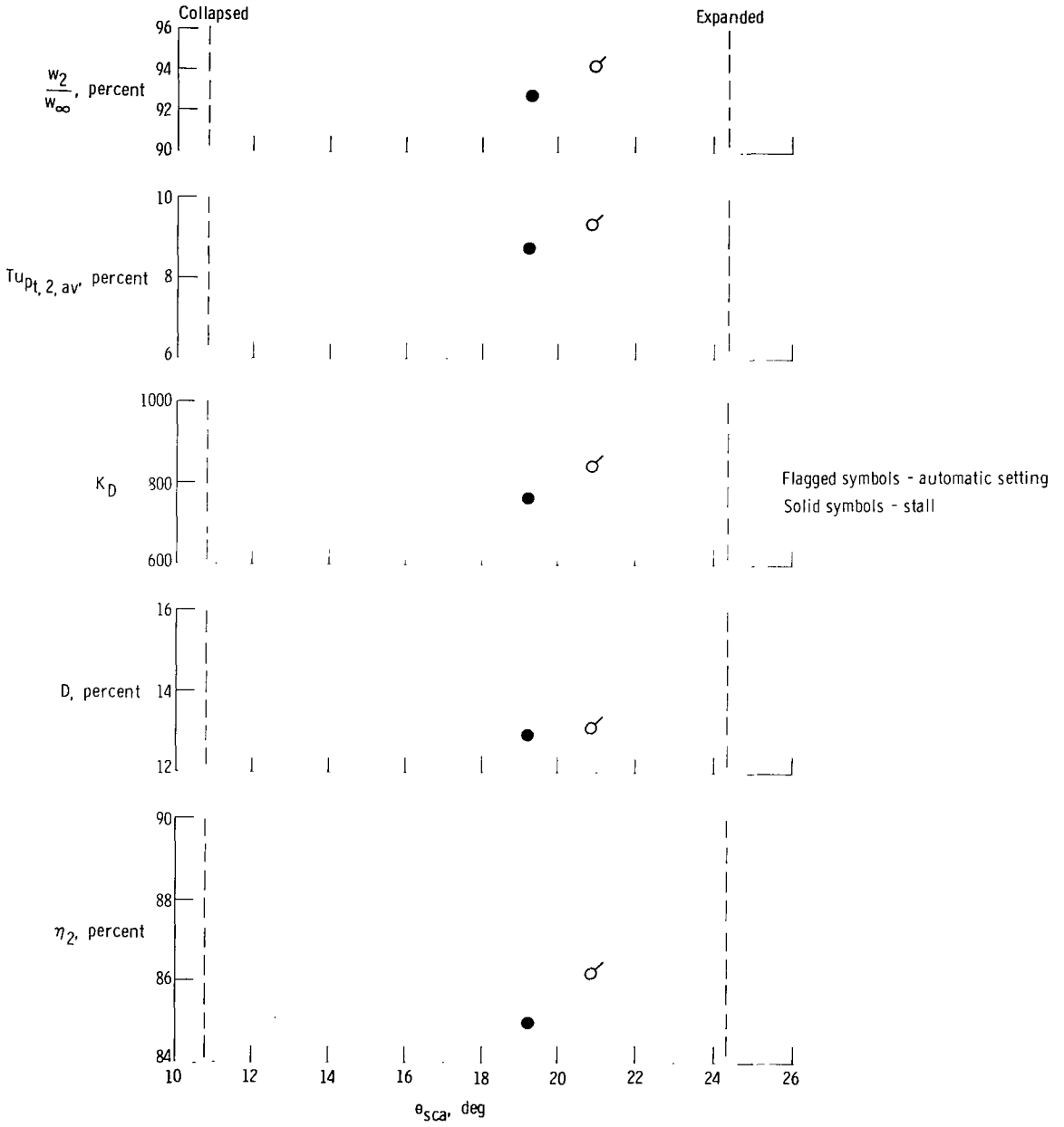

(b) Effect of manual second-cone-angle variation with spike fixed at $\frac{X}{R} = 1.72$.

Figure 15. Concluded.

a more pronounced effect on inlet performance than $\frac{X}{R}$. However, boundary-layer bleed in the region of normal shock impingement on the spike is known to have an appreciable effect on performance (refs. 9 to 11), and therefore the location of the spike bleed holes relative to normal shock position and resultant bleed effectiveness may also have been important. For all supersonic rearward spike movements (figs. 13 to 15), K_D decreases while $Tu_{p_{t,2,av}}$ increases.

Figures 16(a) and 16(b) show the variation in levels of static-pressure turbulence, Tu_{p_s}, at five positions in the inlet with the sharp-lip cowl as well as mean compressor

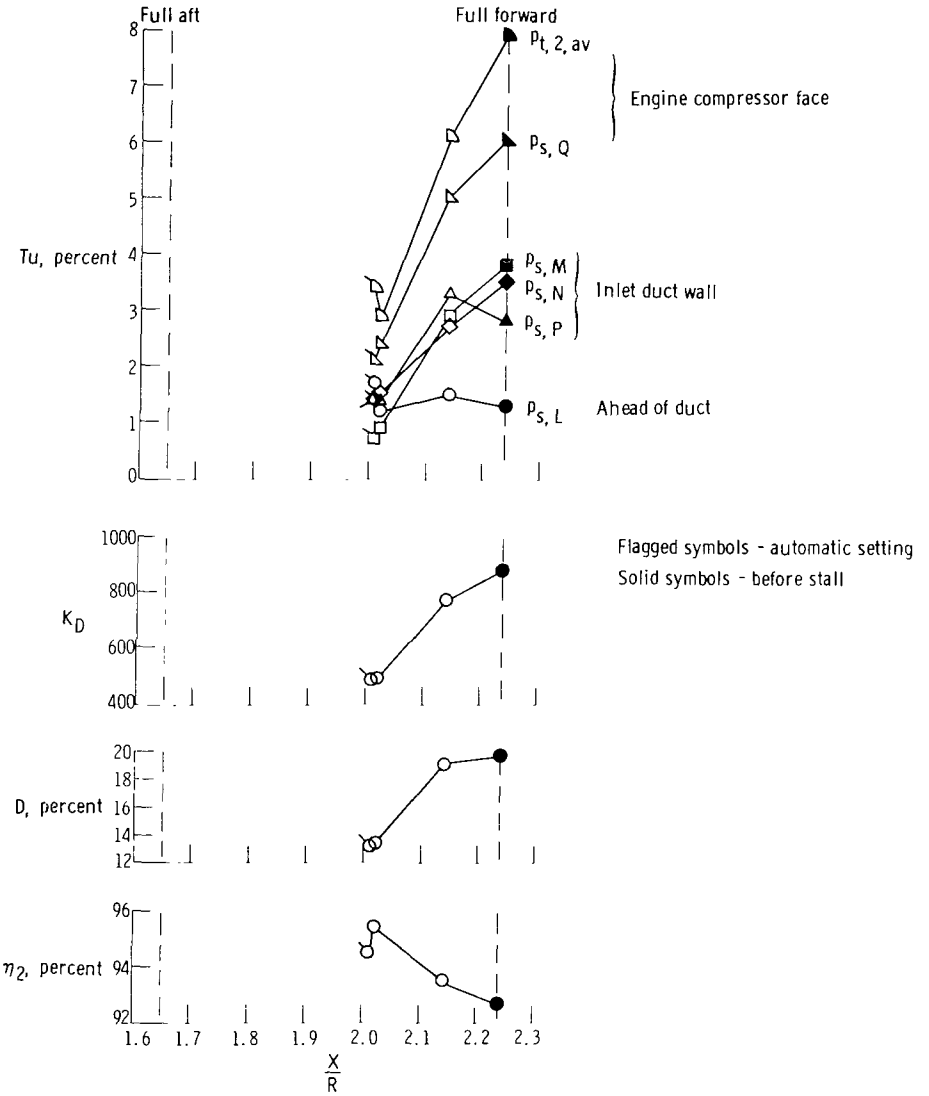

(a) Effect of manual spike movement with second-cone angle fixed, $\theta_{sca} = 13.3^{\circ}$.

Figure 16. Effect of spike position and second-cone angle on duct turbulence and inlet performance with sharp-lip cowl configuration at $\alpha = 3^{\circ}$, $M_{\infty} = 1.3$, and $h = 9150$ meters (30,000 feet).

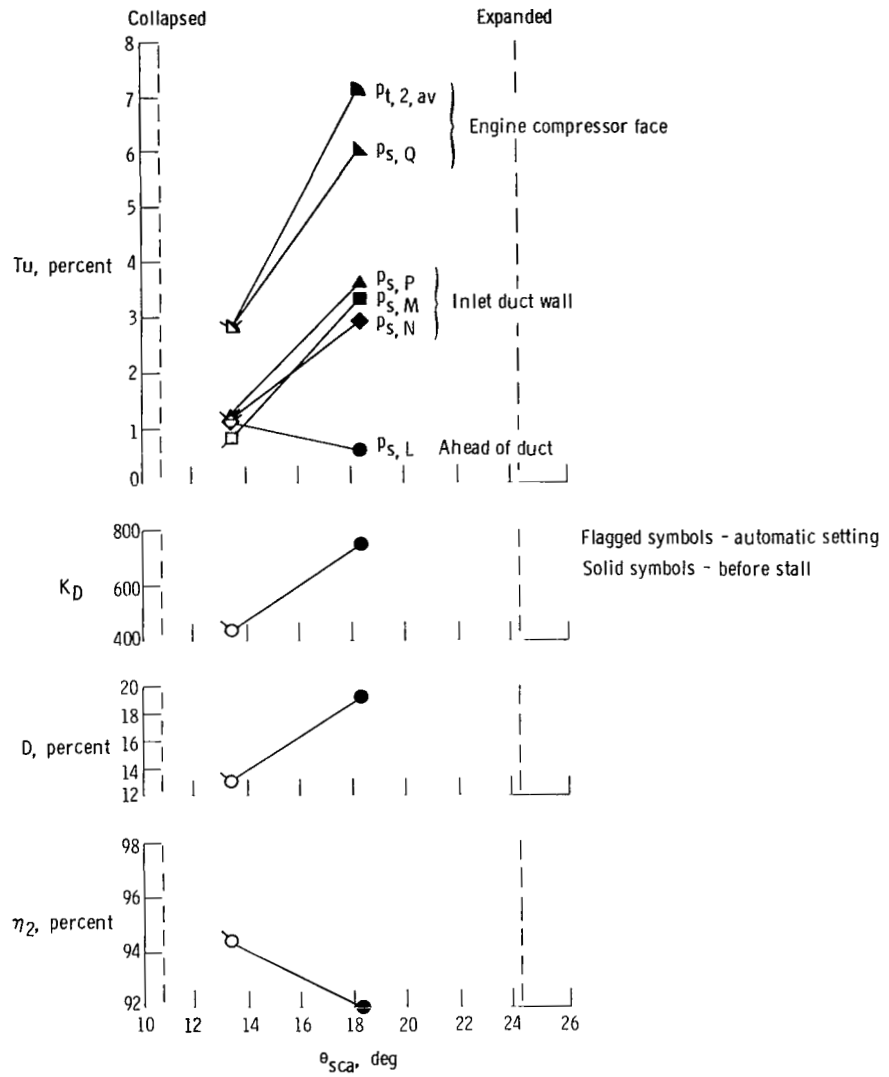

(b) Effect of manual second-cone-angle expansion with spike fixed at $\frac{X}{R} = 2.00$.

Figure 16. Concluded.

face total-pressure turbulence, $Tu_{p_{t,2,av}}$, η_2, D, and K_D during spike and cone maneuvers at $M_\infty = 1.3$, h = 9150 meters (30,000 feet), and $\alpha = 3.0°$. During both maneuvers, the values of the turbulence factors in the duct and at the compressor face more than double the values at the automatic setting, and a $Tu_{p_{t,2,av}}$ value of between 7 percent and 8 percent was measured just prior to the stall. As the air flows over the spike and cone through the duct and into the engine, the level of turbulence generally increases: and, as the spike is translated forward or the cone is expanded, this level of turbulence increases.

Approximate compressor stall boundaries on inlet geometry variations at h = 3050 meters (10,000 feet) and 9150 meters (30,000 feet) are shown in figure 17(a). Similar data at h = 13,700 meters (45,000 feet) are shown in figure 17(b). These

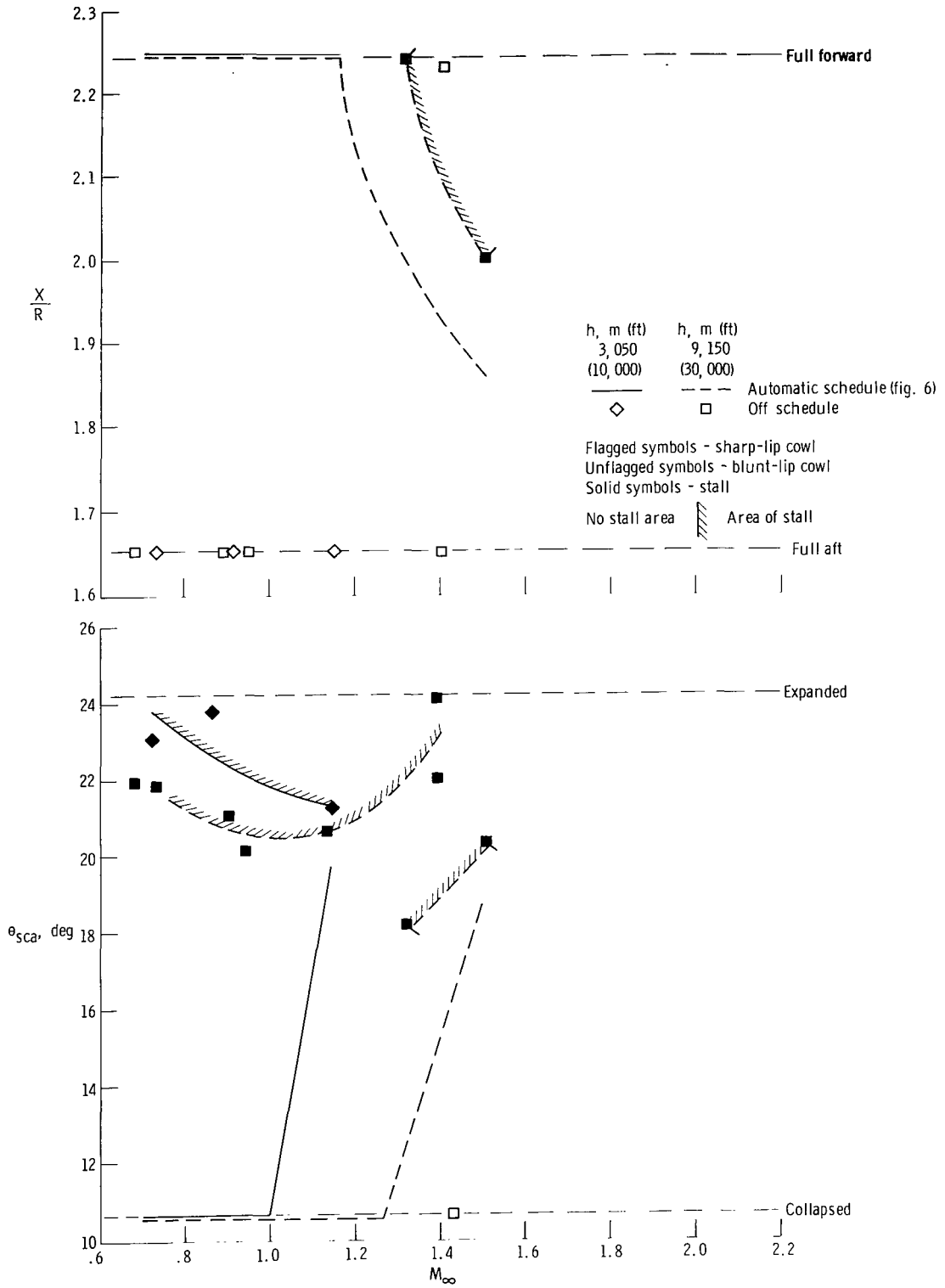

(a) Compressor stall boundaries at h = 3050 meters (10,000 feet) and 9150 meters (30,000 feet).

Figure 17. Flight-determined compressor stall boundaries on off-design spike positions and second-cone angles.

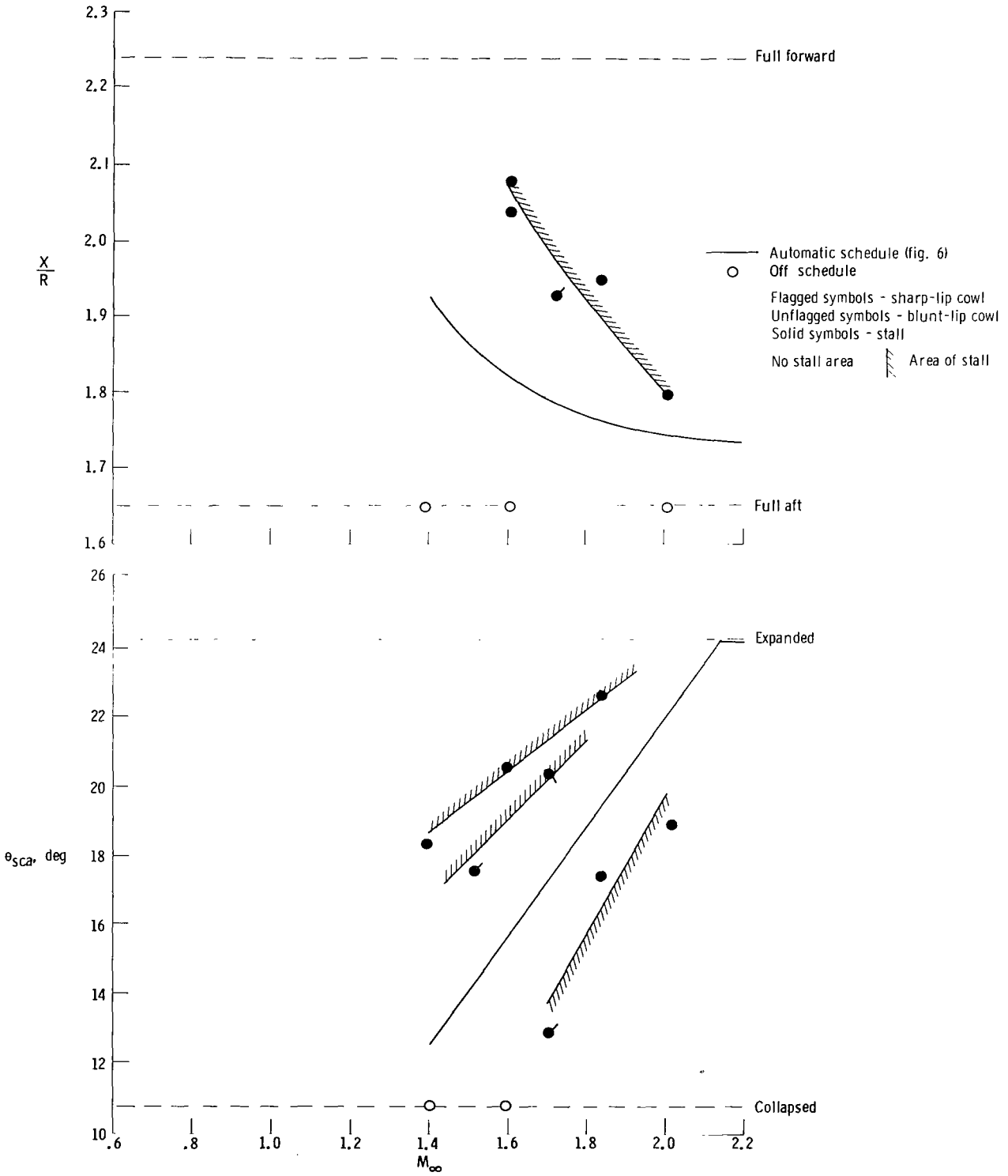

(b) Compressor stall boundaries at h = 13,700 meters (45,000 feet).

Figure 17. Concluded.

boundaries were determined by using spike-position and second-cone-angle data recorded during 41 off-schedule tests, 27 of which resulted in compressor stalls. Each point represents the maximum motion of either variable (up to the time of compressor stall) achieved while the other variable was held fixed in its automatic position. Included for reference is the automatic schedule replotted from figure 6. Stalls were induced at all Mach numbers, but no stalls resulted from rearward spike movements. Furthermore, a wider range of spike positions and second-cone angles was attainable without stall at the subsonic and transonic Mach numbers. This range was restricted above Mach 1.4. It is evident from the second-cone data that more range was available in second-cone angle without causing a compressor stall with the blunt-lip cowl than with the sharp-lip cowl. This result was unexpected because neither cowl resulted in markedly superior performance during automatic inlet testing (fig. 8).

In general, the data presented in this section indicate that near-optimum performance was achieved by the test inlet control system. Off-schedule positioning of the spike and second-cone angle with few exceptions (at high Mach numbers where the compressor stall range was narrowest) resulted in definite performance losses.

Although performance parameters derived from low-response measurements in the test inlet invariably showed performance degradation prior to off-schedule-induced compressor stalls, it is significant that no specific limiting levels in η_2, D, K_D, $Tu_{p_{t,2,av}}$, or $\frac{w_2}{w_\infty}$, for example, were observed consistently. It was found in reference 3, however, that high-response K_D calculations at 400 samples per second correlated with the occurrence of compressor stall in the F-111A test inlet and yielded consistent peak values immediately before compressor stall.

Comparison of Flight and Wind-Tunnel Data

Extensive wind-tunnel developmental tests of the F-111A air-induction system were conducted at Arnold Engineering Development Center (AEDC). Data were selected from a number of reports which resulted from these wind-tunnel programs to obtain the configuration and operating conditions closest to the flight data. These data are compared with flight data in this section.

References 9 and 10 discuss the testing of 1/6-scale models which simulated the inlets, fuselage, and wing gloves ahead of the inlets. These models were of an early configuration of the F-111A airplane, which had sharp-lip cowls, bleed holes in the spike, but no vortex generators in the duct and no instrumentation boom on the airplane nose. Among the objectives of the wind-tunnel tests were evaluation of the effects of spike position and second-cone angle on inlet performance and determination of a preliminary inlet controller schedule.

Figure 18(a) compares model total-pressure recovery, η_2, and distortion, D, from reference 9 as a function of spike position for two second-cone angles at Mach 1.7 with flight data for $M_\infty = 1.6$. Although the flight Mach number is lower than

the wind-tunnel Mach number (the flight automatic schedule in fig. 6 predicts $\Theta_{sca} = 16°$ to $19°$ for $M_\infty = 1.7$), the agreement is reasonable, inasmuch as the trends are similar and η_2 would be expected to be from 1 percent to 2 percent high because of the lower M_∞. (See fig. 8(a).) The flight data show that a compressor stall was induced at a spike position of 2.05.

A second comparison in figure 18(b) at $M_\infty = 2.0$ for both flight and 1/6-scale-model data from reference 9 shows similar trends. The wind-tunnel η_2 data ($\Theta_{sca} = 20°$) have a 1.3 percent higher recovery than the flight η_2 data at the spike and second-cone automatic setting ($\Theta_{sca} = 19.9°$). A compressor stall was encountered in flight at $\frac{X}{R} = 1.8$, as also shown in figure 17(b).

Flight data from figures 18(a) and 18(b) are replotted in figures 18(c) and 18(d) for comparison with data from the 1/6-scale tests reported in reference 10. In both figures the agreement in recovery is reasonable, but a reduction in model inlet distortion resulted in poorer agreement in the distortion data, with the flight data higher in both instances. The compressor stalls observed in flight occur well

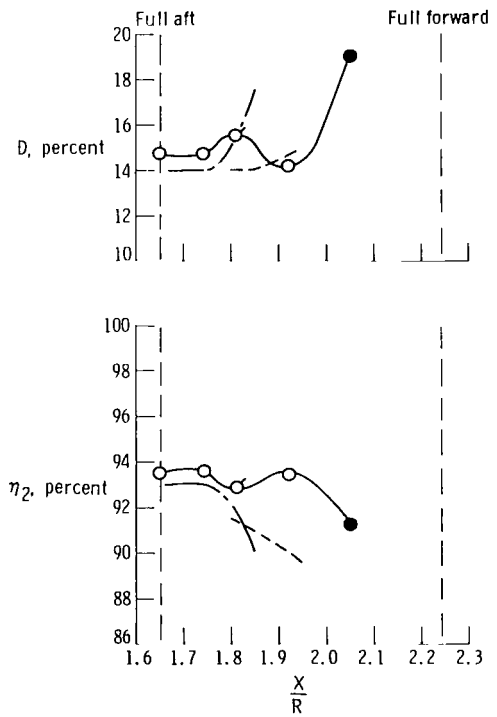

	Flight	1/6-scale wind tunnel (ref. 9)
M	1.6	1.7
h, m (ft)	13,700 (45,000)	---
α, deg	5	5.5
β, deg	0.25	0
θ_{sca}, deg	16	15 and 18
N_{Re}	6.8×10^6	4.83×10^5
Symbol	—○—	– – – – $\theta_{sca} = 15°$ — – – — $\theta_{sca} = 18°$
Cowl configuration	Blunt lip	Sharp lip

Flagged symbols - automatic setting
Solid symbols - stall

(a) Effect of manual spike movement at $M_\infty = 1.6$ to 1.7.

Figure 18. Comparison of off-design inlet performance data from flight and 1/6-scale wind-tunnel tests.

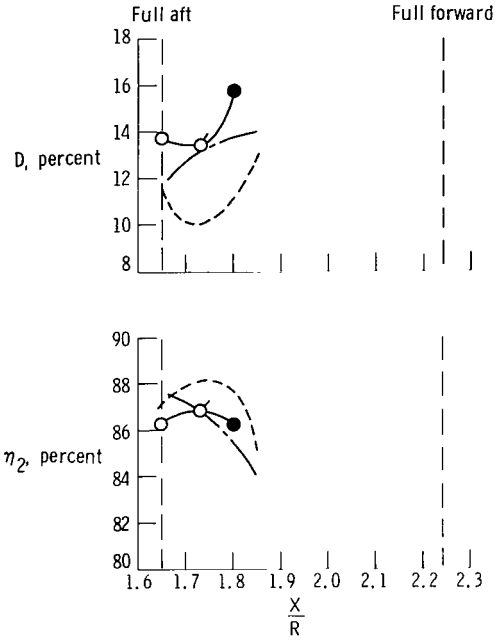

	Flight	1/6-scale wind tunnel (ref. 9)
M	2.0	2.0
h, m (ft)	13, 700 (45, 000)	---
α, deg	4	5.5
θ_{sca}, deg	20.6	18 and 20
N_{Re}	8.48×10^6	6.8×10^5
Symbol	—○—	– – – – $\theta_{sca} = 20°$ — — — $\theta_{sca} = 18°$
Cowl configuration	Blunt lip	Sharp lip

Flagged symbols - automatic setting
Solid symbols - stall

(b) Effect of manual spike movement at $M_\infty = 2.0$.

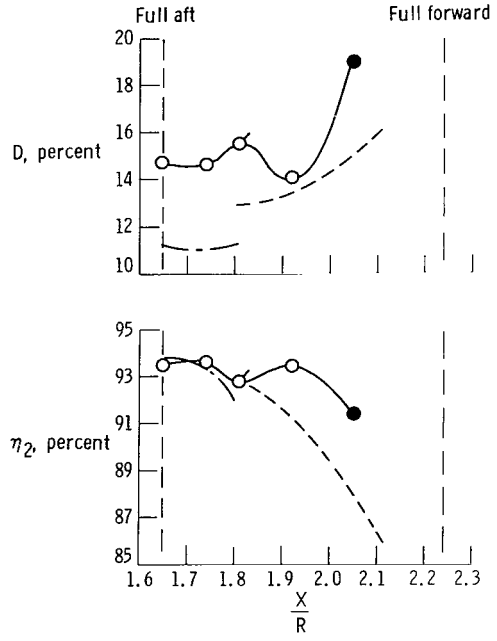

	Flight	1/6-scale wind tunnel (ref. 10)
M	1.6	1.75
h, m (ft)	13, 700 (45, 000)	----
α, deg	5	5.5
θ_{sca}, deg	16	15 and 18
N_{Re}	6.81×10^6	5.06×10^5
Symbol	—○—	– – – – $\theta_{sca} = 15°$ — - — $\theta_{sca} = 18°$
Cowl configuration	Blunt lip	Sharp lip

Flagged symbols - automatic setting
Solid symbols - stall

(c) Effect of manual spike movement at $M_\infty = 1.6$ to 1.75.

Figure 18. Continued.

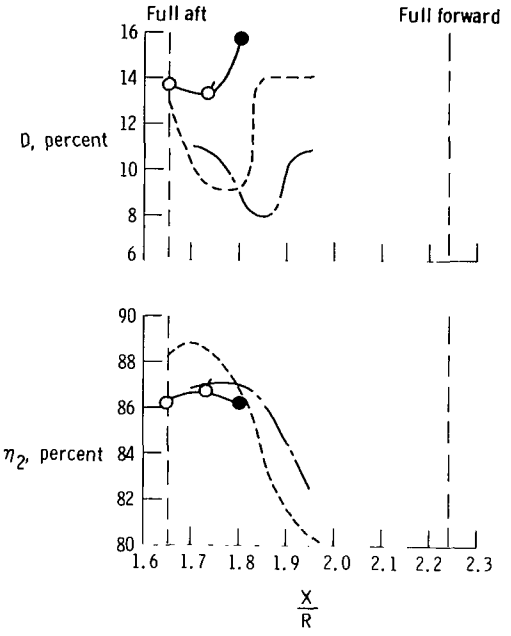

	Flight	1/6-scale wind tunnel (ref. 10)
M	2.0	2.0
h, m (ft)	13,700 (45,000)	---
α, deg	4	5.5
θ_{sca}, deg	20.6	18 and 20
N_{Re}	8.48×10^6	6.8×10^5
Symbol	—○—	- - - θ_{sca} = 20° — - — θ_{sca} = 18°
Cowl configuration	Blunt lip	Sharp lip

Flagged symbols - automatic setting
Solid symbols - stall

(d) Effect of manual spike movement at $M_\infty = 2.0$.

Figure 18. Concluded.

within the range of $\frac{X}{R}$ values tested in the wind tunnel. In figure 18(d) the wind-tunnel distortion curve for $\theta_{sca} = 20°$ shows a valley near the flight automatic setting, $\frac{X}{R} = 1.73$, and an abrupt rise just beyond $\frac{X}{R} = 1.80$, where stall occurred.

Following the 1/6-scale studies, several tests with a full-scale inlet model were conducted in the same tunnel. Reference 11 discusses the inlet performance testing with a variable airflow engine simulator at free-stream Mach numbers from 1.89 to 2.67. Reference 5 describes operational characteristics of the inlet control system and presents control system performance for all phases of the full-scale program. Reference 12 reports results of the inlet-engine compatibility and inlet performance investigation for subsonic and supersonic Mach numbers (M_∞ = 1.89 to 2.20) using an XTF30-P-1 engine. The configuration of the full-scale inlet model used during these tests was essentially the same as the 1/6-scale-model inlet configuration discussed earlier and in references 9 and 10. Although comparison of flight and full-scale model data was limited by differences in Mach number, some of the comparisons that were made are shown in figures 19(a) and 19(b).

Additional 1/6-scale-model tests were performed over the Mach number range from 0.9 to 2.5 at AEDC (ref. 7) in an effort to improve inlet performance obtained during early flight testing of a prototype F-111A aircraft. These tests surveyed proposed modifications to inlet entrance geometry and internal area distribution and the effects of flow stabilizing devices (vortex generators) within the inlet.

The spike positions and second-cone angles selected for optimum performance as

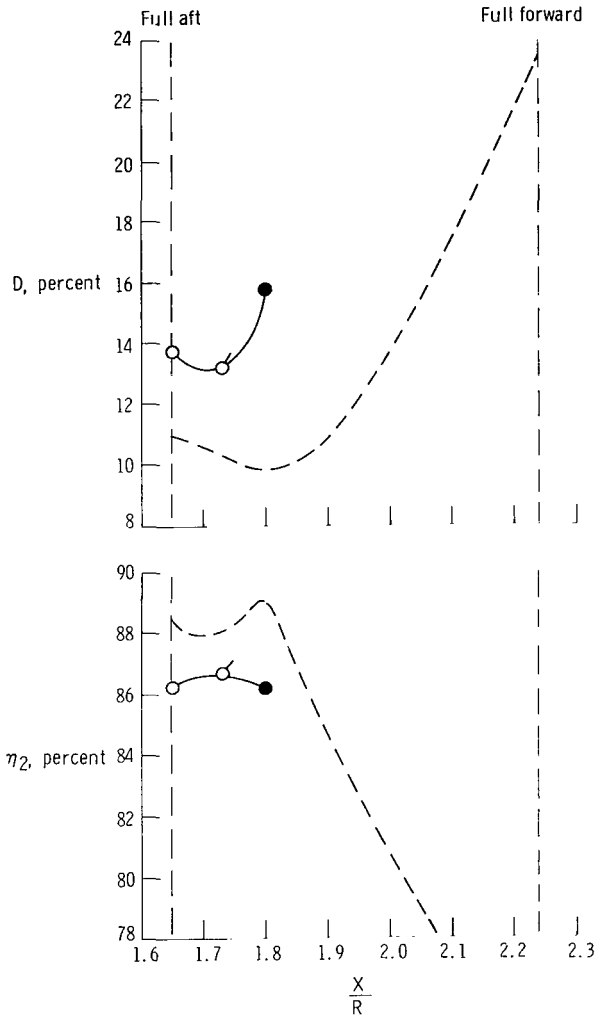

	Flight	Full-scale wind tunnel (ref. 11)
M	2.0	2.0
h, m (ft)	13,700 (45,000)	---
α, deg	4	5.5
θ_{sca}, deg	20.6	20
N_{Re}	8.48×10^6	1.29×10^6
Symbol	—○—	— — —
Cowl configuration	Blunt lip	Sharp lip

Flagged symbols - automatic setting
Solid symbols - stall

(a) Effect of manual spike movement.

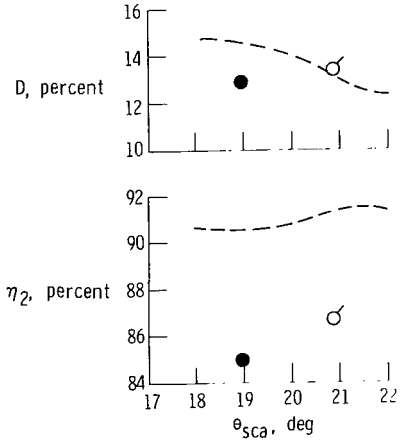

	Flight	Full-scale wind tunnel (ref. 11)
M	2.0	1.89
h, m (ft)	13,700 (45,000)	----
α, deg	5	5.5
X/R	1.72	1.72
N_{Re}	8.48×10^6	1.64×10^6
Symbol	○	— — — —
Cowl configuration	Blunt lip	Sharp lip

Flagged symbols - automatic setting
Solid symbols - stall

(b) Effect of manual second-cone-angle variation.

Figure 19. Comparison of off-design inlet performance data from flight and full-scale wind-tunnel tests.

a result of 1/6-scale-model testing are replotted from reference 7 in figure 20 for comparison with the flight automatic schedule data. As shown, the wind-tunnel data indicate a slightly delayed but more rapid spike retraction and a slightly earlier and less rapid cone expansion at 9150 meters (30,000 feet) (with increasing M_∞) than the flight data. The flight data of figures 13(a), 14(a), and 15(a) indicate small reductions in K_D at the expense of an increase in Tu and a decrease in $\frac{w_2}{w_\infty}$ for spike positions rearward of the automatic setting. The flight data in figures 13(b), 14(b), and 15(b) indicate further that for the flight Mach numbers and altitudes shown a more expanded or more collapsed second cone would be detrimental to performance. However, the wind-tunnel predictions are considered to be reasonable because ample provision for expected adjustment of the

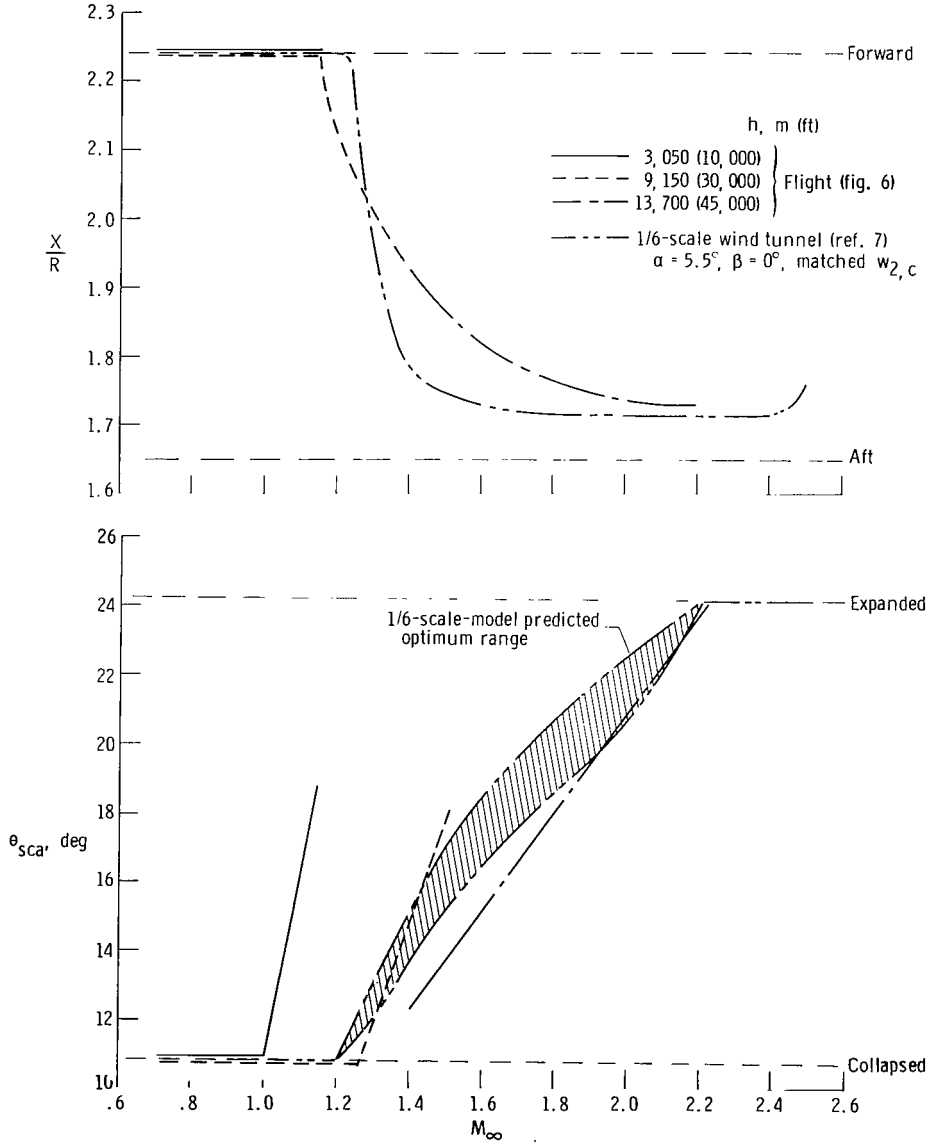

Figure 20. Comparison of flight spike-position and second-cone-angle schedules with 1/6-scale wind-tunnel-model schedules for predicted optimum performance.

spike-position and second-cone-angle schedules were built into the inlet controller to accommodate flight-test results.

One-sixth-scale-model total-pressure recovery and distortion data for matched engine airflow and optimum $\frac{X}{R}$ and θ_{sca} from references 7, 9, and 10 are summarized in figures 21(a) and 21(b) for comparison with flight mean recovery and distortion data from figure 8. The differences between flight and wind-tunnel η_2 over the Mach number range of the comparison in figure 21(b) are no greater than about 3 percent; the wind-tunnel data appear to be conservative below and optimistic above Mach 1.5.

In general, limited comparisons of F-111A flight inlet performance data (η_2 and D) with both full-scale and 1/6-scale-model data have frequently shown similar trends during off-schedule operation with differences in absolute values of total-pressure recovery within about 3 percent.

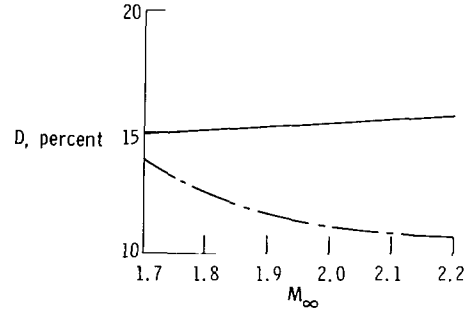

(a) Total-pressure distortion.

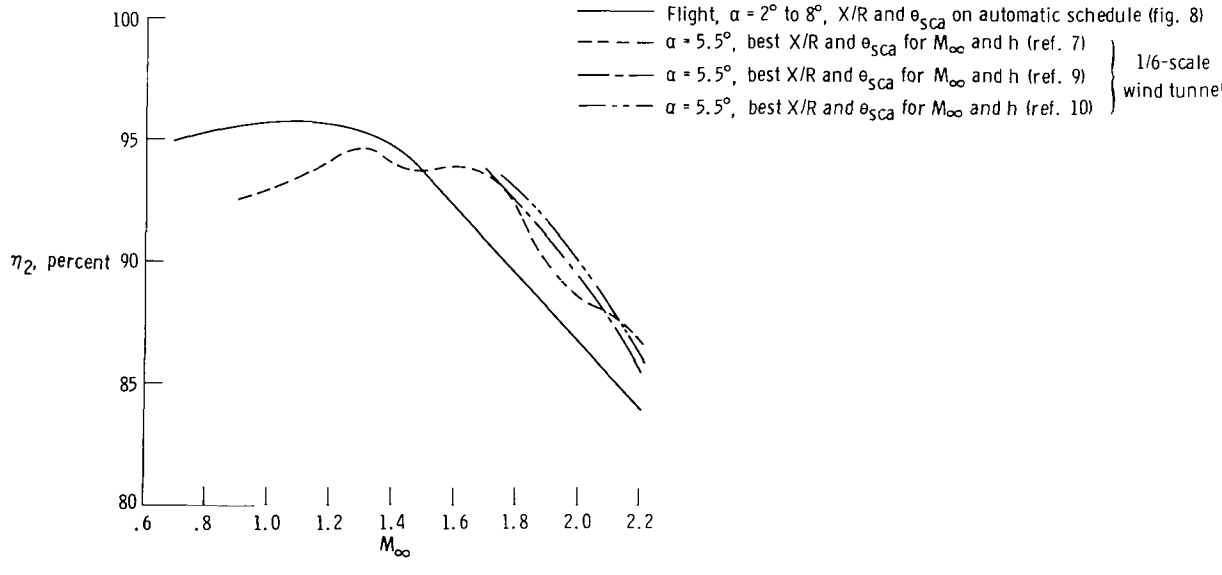

(b) Total-pressure recovery.

Figure 21. Comparison of flight inlet performance during automatic control with 1/6-scale-model optimum performance.

SUMMARY OF RESULTS

Flight-test data were obtained from the left inlet of a prototype version of the F-111A airplane during automatically scheduled and manual off-schedule positioning of the compression spike and second-cone angle at Mach numbers from 0.68 to 2.18. The flight-test data showed that a relatively wide range in inlet performance parameters such as total-pressure recovery and distortion may be expected during normal operation of an inlet and control system of the type used for this study. In addition, at an altitude of 13,700 meters (45,000 feet) second-cone-angle data showed as much as ±1.5° of scatter while the inlet geometry controller was functioning properly and yielding near optimum inlet performance. However, such variations in geometry were observed to be less tolerable with increasing Mach number because of the increase in inlet-generated flow distortion and the possibility of compressor stall.

Specifically, data analysis and limited comparisons with wind-tunnel-model data yielded the following results:

(1) Automatic variation of the inlet geometry variables of spike position and second-cone angle according to inlet Mach number measurements and a preset schedule produced nearly optimum performance for the test installation in terms of total-pressure recovery, total-pressure-distortion indices, turbulence parameter, and mass-flow ratio.

(2) Off-schedule operation resulted in significant reductions in total-pressure recovery and mass-flow ratio and increases in the total-pressure-distortion indices and turbulence factor. Second-cone expansion and rearward spike movement were found to be most and least detrimental to inlet performance, respectively.

(3) As a result of small movements in spike position and second-cone angle, the test F-111A engine was more likely to experience a compressor stall at high supersonic Mach numbers than at subsonic and low supersonic Mach numbers.

(4) Off-schedule second-cone angles at fixed spike positions could be varied over a wider range with the blunt-lip cowl without compressor stall than with the sharp-lip cowl.

(5) Off-schedule F-111A inlet performance data in terms of total-pressure recovery and distortion showed trends similar to those of both full-scale and 1/6-scale-model data. Also, total-pressure recovery obtained during automatic operation of the test inlet compared within about 3 percent of 1/6-scale-model data for predicted optimum inlet geometry.

Flight Research Center,
National Aeronautics and Space Administration,
Edwards, Calif., May 10, 1971.

APPENDIX A

INLET CONFIGURATION DETAILS OF THE F-111A TEST AIRPLANE

Splitter Plate

The splitter plate was positioned forward of the inlet between the fuselage and the inlet to prevent the spike-generated conical and normal shocks from interacting with the fuselage boundary layer (fig. 4(a)). The splitter plate was also designed as a subinlet to remove the fuselage boundary-layer air and thus prevent it from entering the inlet. Part of this air was diverted downward and discharged below the inlet; the remainder passed through and cooled the engine compartment, then exited at the rear end of the airplane around the engine nozzle. The distance between the splitter plate and the fuselage was 8.26 centimeters (3.25 inches) at the top and 16.5 centimeters (6.50 inches) at the bottom. The plate extended approximately 1.2 meters (4.0 feet) ahead of the inlet and about 0.3 meter (1.0 foot) below.

Subinlets

Two additional subinlets were available to remove the low-energy boundary-layer air (fig. 4(a)). One of the pie-shaped subinlets was designed to remove the boundary-layer buildup on the splitter plate. This low-energy air merged with the air removed by the splitter plate and was used for engine compartment cooling. The other pie-shaped subinlet was designed to remove the boundary-layer buildup on the under-side of the wing glove. This low-energy air was vented overboard to the rear of the inlet and under the wing.

Spike

The air compression surfaces of the inlet "spike" were comprised of two cones. The first cone, selected for low spillage drag at a Mach number of 1.2, had a fixed semivertex angle of 12.5°. The second cone was perforated to provide boundary-layer bleed in the region of normal shock impingement, and the angle of the second cone, Θ_{sca}, was expandable from 10.8° to 24.3° with respect to the inlet centerline. The entire centerbody cone system, or spike, was capable of translating from a full forward position where $\frac{X}{R} = 2.24$ to a full rearward position where $\frac{X}{R} = 1.65$. Thus, the inlet variables were spike position, $\frac{X}{R}$, and second-cone angle, Θ_{sca}.

Cowl Configurations

Two different cowl configurations were used during the flight tests. One had a relatively sharp leading edge, and the other had a more rounded lower lip contour, or blunt leading edge, for reduced separation at low speeds and high angles of attack. Figures 4(a) to 4(d) show the blunt-lip cowl configuration, and figure 4(e) shows the sharp-lip configuration. The cowls were also designed to translate forward to open a 15-centimeter- (6.0-inch-) wide, vertical, faired gap to provide additional engine airflow

during ground operation, takeoff, and low-speed flight. The cowl lip radius of 84.56 centimeters (33.29 inches) was used for both configurations.

Vortex Generators

Vortex generators were installed at three locations in the subsonic diffuser to reduce boundary-layer separation in regions of high area gradient. The generators are shown in figures 4(a), 4(b), 4(c), 4(e), and 5.

APPENDIX B

CALCULATION OF INLET PERFORMANCE PARAMETERS

The equations used to calculate total-pressure recovery, compressor face total-pressure distortion, total-pressure distortion factor, engine and compressor face airflow, and turbulence factor are presented in this appendix.

Total-pressure recovery:

$$\eta = \frac{p_t}{p_{t,\infty}}$$

and

$$\eta_2 = \frac{p_{t,2,av}}{p_{t,\infty}}$$

where

$$p_{t,2,av} = \frac{1}{20} \sum_{j=1}^{20} p_{t,2,j}$$

Compressor face total-pressure distortion:

$$D = \frac{\left(p_{t,2,max} - p_{t,2,min}\right)}{p_{t,2,av}}$$

Total-pressure distortion factor:

$$K_D = \frac{\sum_{i=\text{ring } 1}^{5} \left\{ \left[\frac{\left(p_{t,2,av} - p_{t,2,min}\right)}{p_{t,2,av}} \right]_i \bar{\phi}_i C_i \right\} 100}{\sum_{i=\text{ring } 1}^{5} C_i}$$

Engine airflow:

$$w_2 = w_{2,c} \frac{\delta_2}{\sqrt{\theta_2}}$$

where $w_{2,c}$ was obtained from the engine manufacturer's airflow curves.

APPENDIX B

Free-stream airflow:

$$w_{\infty} = \frac{f(M_{\infty})(p_{t,\infty})\,A_1}{\sqrt{T_{t,\infty}}}$$

where $f(M_{\infty})$ is a tabulated function of M_{∞} from reference 13, in which $p_{t,\infty}$ is expressed in atmospheres, $T_{t,\infty}$ is expressed in °R, and $A_1 = 5.83\ ft^2$.

Turbulence factor:

$$Tu = \frac{6\sigma}{p_{t,2,av}}$$

where

$$\sigma = \left(\psi^2 - \mu^2\right)^{1/2}$$

$$\psi^2 = \frac{1}{n}\sum_{j=1}^{n} p_j{}^2$$

$$\mu^2 = \left(\frac{1}{n}\sum_{j=1}^{n} p_j\right)^2$$

REFERENCES

1. Smith, Ronald H.; Bellman, Donald R.; and Hughes, Donald L.: Preliminary Flight Investigation of Dynamic Phenomena Within Air Breathing Propulsion Systems of Supersonic Aircraft. AIAA Paper No. 68-593, 1968.

2. Bellman, Donald R.; and Hughes, Donald L.: The Flight Investigation of Pressure Phenomena in the Air Intake of an F-111A Airplane. AIAA Paper No. 69-488, 1969.

3. Burcham, Frank W., Jr.; and Hughes, Donald L.: Analysis of In-Flight Pressure Fluctuations Leading to Engine Compressor Surge in an F-111A Airplane for Mach Numbers to 2.17. AIAA Paper No. 70-624, 1970.

4. Mechtly, E.A.: The International System of Units - Physical Constants and Conversion Factors. NASA SP-7012, 1969.

5. Herron, R.D.; and Davis, R.E.: Wind Tunnel Investigation of an Inlet Geometry Control System in a Full-Scale F-111 Inlet Model. AEDC-TR-65-53, Arnold Eng. Dev. Center, March 1965.

6. Ames Research Staff: Equations, Tables, and Charts for Compressible Flow. NACA Rep. 1135, 1953. (Supersedes NACA TN 1428.)

7. Hartin, J.P.: Wind Tunnel Investigation at Transonic and Supersonic Mach Numbers of Duct Modifications to the F-111A Inlet. AEDC-TR-66-19, Arnold Eng. Dev. Center, Feb. 1966. (Available from DDC as AD 369494.)

8. Re, Richard J.; and Wilmoth, Richard G.: Performance of an External Compression Inlet of a Variable-Sweep Tactical Fighter Model at Mach Numbers From 0.5 to 1.3. NASA TM X-1576, 1968.

9. Herron, R.D.: Wind Tunnel Investigation of a 1/6-Scale F-111 Inlet From Mach Numbers 1.70 to 2.5. Phase III. Tech. Doc. Rep. No. AEDC-TDR-64-88, Arnold Eng. Dev. Center, May 1964. (Available from DDC as AD 349887.)

10. Prunty, C.C.: Wind Tunnel Investigation of a 1/6-Scale F-111 Inlet From Mach Numbers 1.75 to 2.50. Phase IV. Tech. Doc. Rep. No. AEDC-TDR-64-177, Arnold Eng. Dev. Center, Sept. 1964. (Available from DDC as AD 353274.)

11. Daniel, Brady R.: Wind Tunnel Investigation of a Full-Scale F-111 Inlet From Mach Numbers 1.89 to 2.67. Tech. Doc. Rep. No. AEDC-TDR-64-282, Arnold Eng. Dev. Center, Jan. 1965.

12. Hartin, J.P.: Wind Tunnel Investigation of a Full-Scale F-111 Propulsion System at Subsonic and Supersonic Mach Numbers. AEDC-TR-65-61, Arnold Eng. Dev. Center, March 1965.

13. Kerr, H.C.: Mach Number Tables ($\gamma = 1.4$) With Correction Factors for Real Air. CM 1036-1, Ordnance Aerophysics Lab. (Daingerfield, Tex.), General Dynamics, April 9, 1964. (Available from DDC as AD 624598.)

NASA-Langley, 1971 — 2 H-654

005 001 C1 U 02 710827 S00903DS
DEPT OF THE AIR FORCE
AF SYSTEMS COMMAND
AF WEAPONS LAB (WLOL)
ATTN: E LOU BOWMAN, CHIEF TECH LIBRARY
KIRTLAND AFB NM 87117

"The aeronautical and space activities of the United States shall be conducted so as to contribute . . . to the expansion of human knowledge of phenomena in the atmosphere and space. The Administration shall provide for the widest practicable and appropriate dissemination of information concerning its activities and the results thereof."

—NATIONAL AERONAUTICS AND SPACE ACT OF 1958

NASA SCIENTIFIC AND TECHNICAL PUBLICATIONS

TECHNICAL REPORTS: Scientific and technical information considered important, complete, and a lasting contribution to existing knowledge.

TECHNICAL NOTES: Information less broad in scope but nevertheless of importance as a contribution to existing knowledge.

TECHNICAL MEMORANDUMS: Information receiving limited distribution because of preliminary data, security classification, or other reasons.

CONTRACTOR REPORTS: Scientific and technical information generated under a NASA contract or grant and considered an important contribution to existing knowledge.

TECHNICAL TRANSLATIONS: Information published in a foreign language considered to merit NASA distribution in English.

SPECIAL PUBLICATIONS: Information derived from or of value to NASA activities. Publications include conference proceedings, monographs, data compilations, handbooks, sourcebooks, and special bibliographies.

TECHNOLOGY UTILIZATION PUBLICATIONS: Information on technology used by NASA that may be of particular interest in commercial and other non-aerospace applications. Publications include Tech Briefs, Technology Utilization Reports and Technology Surveys.

Details on the availability of these publications may be obtained from:

SCIENTIFIC AND TECHNICAL INFORMATION OFFICE

NATIONAL AERONAUTICS AND SPACE ADMINISTRATION

Washington, D.C. 20546